UNITED NATIONS UNIVERSITY
UNU-GTP
Geothermal Training Programme

Orkustofnun, Grensasvegur 9,
IS-108 Reykjavik, Iceland

Reports 2016
Number 22

METHODOLOGY FOR OPTIMIZING PIPELINE ROUTE SELECTION, SEPARATOR AND POWER PLANT PLACEMENT IN GEOTHERMAL PROJECTS – CASE OF OLKARIA IV IN KENYA

Harrison Kiplimo Keter
Kenya Electricity Generating Company, Ltd. - KenGen
P.O. Box 785-20117
Naivasha
KENYA
kketer@kengen.co.ke

ABSTRACT

The objective of this study is to create a tool and develop a methodology for optimizing pipeline route selection, placement of separators and power plants in geothermal projects. The process usually faces a number of constraining challenges including environmental protection issues, land use policies and technical requirements. Among the technical constraints considered are pressure drop along the pipeline, flow regimes, pipeline diameter, thickness and length, maximum allowable gradients and associated costs for each component. The pipe diameter, thickness and overall length have a great bearing on the total pipeline cost. An optimized route and pipe diameter will directly lead to an optimized project cost that is the drive for this study.

Variable topography distance transform (VTDT) method was used to define the routes and weighted variable topography distance transform (WVTDT) to find best location for the separators and the power plant. Application of constraints was used to optimize the pipe network and flow in each pipe. VTDT is based on the chamfer metric distance transform algorithm which works with the digital elevation matrix (DEM) to get height values for each cell. For this study the DEM and field data for Olkaria IV geothermal field were used to test the model. The study has shown that good results are obtained with VTDT for route selection, separator and plant location optimization. The study also proposes a sequence of optimization steps where the separator location is first optimized taking into account the location of production wells and hot reinjection wells. Cold reinjection wells are not considered since the pipes are usually made of polyethylene whose price is much lower compared to the price of steel used for other pipelines. The length of the routes from each well to the separator is then determined. This is followed by optimizing the plant location considering the already optimized separator locations. In this study, the use of WVTDT shows that the length of the pipeline can be shortened by 1542 m. It is, however, important to conduct a detailed survey of the area to map out all the coordinates of the no-go zones as defined by human, technical or environmental constraints for inclusion in the program as constraints.

1. BACKGROUND

1.1 Geothermal energy in Kenya

Geothermal resources in Kenya are mainly found along the Kenyan Rift Valley with the exception of a few areas outside of the rift having been mapped that contain geothermal resources. Some of the areas mapped out of the rift system are Masa Mukye located in the coast region and around Homa Hills in the Nyanza province in the west of the country. Figure 1 shows the geothermal areas of Kenya which have been mapped. The rift system is characterized by striking structural and topography features trending in north-south direction through central Kenya (Riaroh and Okoth, 1994). Various studies which have been conducted indicate the presence of near surface heat sources. The Kenyan government has prioritized the exploitation of the geothermal resource as a main source of energy. The greater Olkaria geothermal field is located in the Kenya Rift Valley, about 120 kilometres northwest of Nairobi, covering more than 200 square kilometres. It is the largest exploited geothermal field in Africa with over 600 megawatts (MWe) of developed power (August 2016). The field is home to Olkaria I, II, III and IV power plants and fifteen wellhead plants developed and operated by Kenya Electricity Generating Company (KenGen). The wellhead or modular plants together generate a total of 81.1 MW. According to KenGen internal reports in 2012, the development of Olkaria V and VI power plants are at advanced stages with planned operational timelines of 2017 and 2018, respectively (Mannvit, 2012). There are intentions to further develop Olkaria VII, VIII, IX and X within the Olkaria field. Olkaria V and VI each require a total of 45 wells to avail required steam. In June 2016, 43 and 41 wells had been drilled in Olkaria V and VI respectively. The next stage will include steam field development and power plant construction. The Olkaria field is surrounded by further geothermal prospects such as Suswa and Longonot.

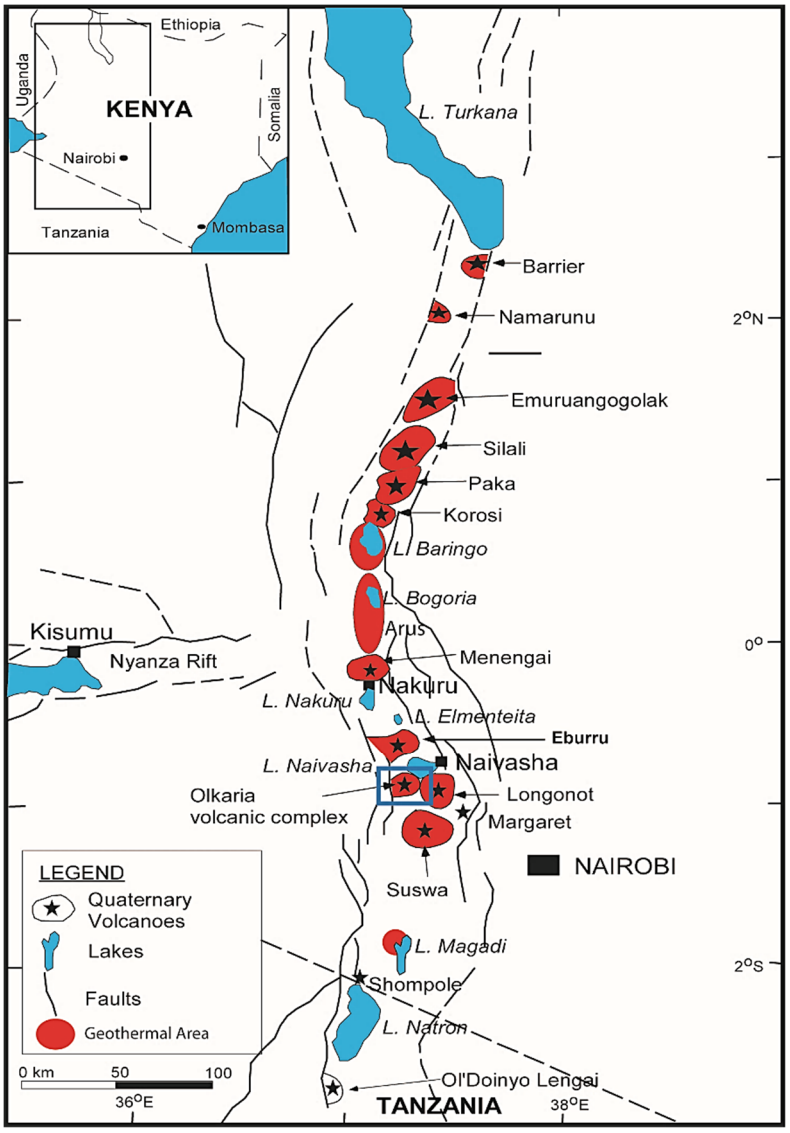

FIGURE 1: Geothermal prospects in the Kenyan rift (Mwawongo, 2013)

In order to fast track geothermal development, the government of Kenya has created a conducive policy framework that encourage private sector investments. This has resulted in three private developers being granted licences to develop geothermal energy in Olkaria, Akiira and Longonot fields. Drilling in Longonot and Akiira is on-going and the plans for development very alive. This study considers a case study of Olkaria IV geothermal field. However, the results can be used to inform planning and decision making processes for development in other areas.

1.1.1 General layout of Olkaria IV geothermal field

The Olkaria IV geothermal field is part of the greater Olkaria geothermal field in Kenya. It covers an area of approximately 25 square kilometres. The field has been developed and Olkaria IV power plant in this field currently produces 140 MWe. The field has a total of 30 wells drilled, 21 of which are production wells, while 7 are hot re-injection wells and two are cold reinjection wells. A total of 4 separator stations are used in the field. Figure 2 shows a schematic diagram of the location of various systems in the Olkaria IV field. The study has used data from this field to test the model.

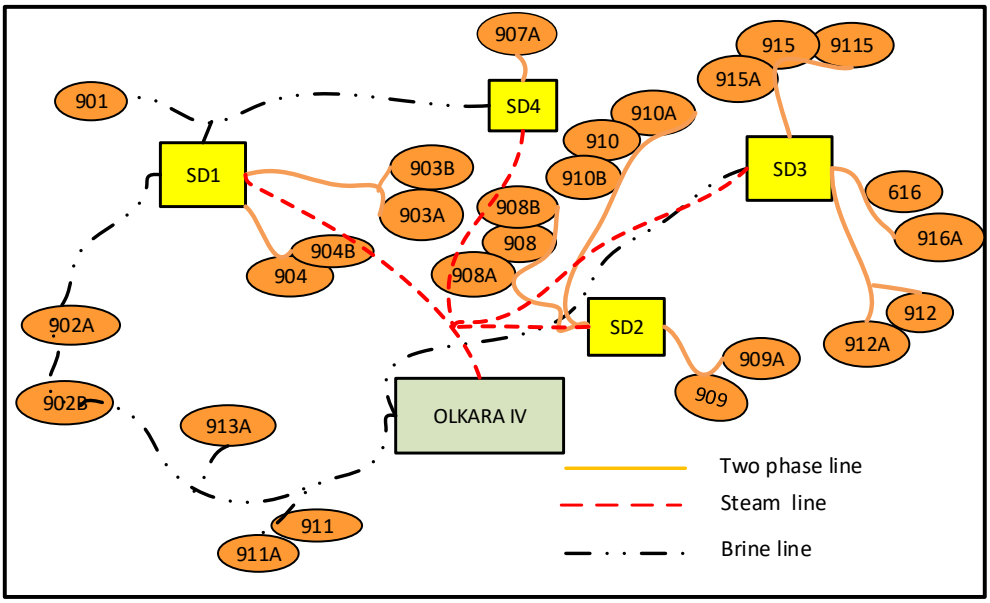

FIGURE 2: Schematic drawing of Olkaria IV geothermal field

1.2 Motivation

Geothermal energy is fast taking a leading role in the generation of electricity in Kenya. In the future plan Vision 2030, the government has set the target of 5000 MWe by the year 2030 out of which over 2000 MWe will come from geothermal energy (GoK, 2014). Among other companies in the energy sector in the country, KenGen has the obligation of generating 700 MWe. The company has generated additional 300 MWe in the last two years (2014-2015) in Olkaria geothermal field and has an ambitious plan for more power production in the same field. In March 2016, wells providing steam for about 280 MWe had already been drilled and more drilling work continues. The steam system forms part of the critical sections of the geothermal power generation, contributing about 10% of the overall cost of geothermal field development (Onyango, 2015). The optimization of pipeline routes, separator and power plant placement is essential for managing the steam gathering system cost. In order to achieve this, a tool is required to guide the company in designing and sizing such systems. Current practice is to propose preliminary routes and separator stations by experienced staff before engaging consultants. This can be subjective depending on individual's judgement. Therefore there is need for a structured way of doing this kind of work, which forms the basis of this study. The objective of the study presented is to develop a decision making tool to be used to optimize pipeline routes, separator and power plant placement. The initial inputs for the model include the digital elevation matrix (DEM), location of wells using global positioning system (GPS), mass output from wells and plant location. In this project the model is tested with data from Olkaria IV geothermal field in Kenya and with improvements it can be used to guide designs and for budgetary planning purposes within Olkaria fields and any other new geothermal fields.

1.3 Objectives of the study

The main objective of this study is to develop a tool for route selection, placement of separators and power plant in order to optimize the steam system. Specifically, the tool will be used for the following:

I. Define the route of a pipeline using weighted variable topography distance transform (WVTDT) - using Olkaria IV as an example;
II. Determine the best location for the separators;
III. Determine the best location of the power plant and compare with the existing location;
IV. Dimensional design of the pipeline and separators; and
V. Determine the preliminary cost for the various systems.

1.4 Scope of the study

This study covers development of an optimization tool for pipeline route selection, design and placement of separator stations and location of power plant. Data from Olkaria IV geothermal field in Kenya is used for the case study to analyse and compare results. The steam field system considered in this design is equipped with pipelines connecting eight production wells currently serving separation station (SD2) and a steam pipeline that runs from the separation station (SD2) to the power plant. The separated brine pipeline from the separator station (SD2) to the hot re-injection wells and steam lines from all separators to the optimized plant location are also considered. For the reinjection system, only hot reinjection wells serving SD2 are considered. The works done include selection and optimization of pipeline routes, pipeline and separator design. The cost of the steam system is determined based on Olkaria IV field data presented. Mechanical stress analysis and thermal analysis, while important, are not considered in this report.

2. LITERATURE REVIEW

2.1 Geothermal power plants

In geothermal power production, vapour is required to drive turbines for generating electricity. This vapour is derived directly from naturally occurring vapour which derives its energy from the natural heat of the earth's crust. Geothermal power plants can be broadly categorized into steam power plants mostly located in fields with high enthalpies and binary plants largely found in fields with low enthalpies. High temperature fields with bad chemistry can also be used to feed binary plants. In some areas however, very high temperatures have been found but no fluids are present to transport the heat, instead they have hot dry rocks with very high temperatures. In such areas, the rocks can be fractured and fluids are pumped down to pick up the heat and then pumped up again. These systems are referred to as enhanced geothermal systems and have not been widely developed.

Steam power plants can further be grouped into *direct steam plants* and *flash steam plants* and they can be single flash, double flash or triple flash systems. Dry (direct) steam power plants are built in vapour dominated reservoirs which are characterized by dry saturated or superheated steam. The pressures are constant and above atmospheric, largely controlled by the predominantly continuous steam phase.

In the flash power plants steam is separated from two-phase geothermal fluid in one or several separators depending on the type of plant. Fluids in single flash plants undergo a separation process after which the separated steam is sent to the turbine while the separated brine is directed to a reinjection well. In the double flash cycle systems on the other hand, there is high pressure and low pressure separation. Generally, flash power plants are similar to fossil fuel power plants except for the characteristic that

steam is at saturated state when entering the turbine. Fossil plants may have superheated steam up to temperatures imposed by turbine blades material limits (Nag, 2008).

Binary cycles are installed for temperatures below 180°C and they make use of a secondary working fluid with a low boiling point in a closed power generation cycle. A heat exchanger is used to transfer heat from the geothermal fluid to the working fluid, and the cooled brine is then rejected to the environment or re-injected. The Organic Rankine Cycle (ORC) is commonly used in binary cycle plants and examples are of use of the Kalina cycle. The decision on which type of plant to build in a particular location is depended on the nature of the resource and its properties. In all the cases, a steam line must be constructed between the well and the plant. The design of the pipelines and separation stations is critical to minimize losses along the line and to ensure high efficiencies.

2.2 Geothermal steam gathering system

The steam gathering system in a geothermal power plant is used for collection and transportation of steam from the well head and delivering it to the turbine inlet in the desired condition. It comprises of the following major components: the well, silencers, steam delivery pipeline and expansion loops, flashers, valves, separator stations, gas ejectors and associated auxiliaries. The pipelines can be single-phase or two-phase fluid pipelines depending on the geofluid conditions and designs in place.

Separator stations can be located near the well head or close to the turbine, both possibilities have their merits and demerits. They can also be separate for each well head or centrally placed to serve a number of well heads combined. The selection of separator pressure is very critical for a power plant. If the well head pressure is low, boiling may occur in the formation around the well, which may lead to scaling within the cracks and thus narrow flow passages in the formation. This will lead to short well life. Higher separation pressure means that better steam is available for the turbine (higher enthalpy), but the amount will be less, dictated by separator energy balance as well as productivity due to higher wellhead pressure. This may also influence the separation of non-condensable gases from the geothermal fluid (Valdimarsson, 2010).

Therefore, the selection of the separator pressure is an optimization process. According to DiPippo (2007) the best choice will be determined by the economics taking into account site-specific conditions including temperature, pressure and chemical nature of geofluid, well distribution (both production and reinjection wells) relative to the powerhouse location, topography of the site, and method of fluid disposal, including any required scale control technique. Generally, the efficiency of the entire gathering system will be determined by careful placement and design of all parts.

2.3 Geothermal steam system optimization

Steam system optimization implies the selection of steam routes and placement of separator stations and auxiliary equipment to ensure delivery of steam in the right quality to the turbine with minimal pressure drop and cost of the system. The shortest route usually should be the cheapest. However, large diameters and other constraints along the route may make the route expensive or not practical. The optimal route therefore takes into consideration all the constraints in the field like technical issues, environmental or even administrative restrictions. Different approaches have been developed for route selection and optimization for different applications like transportation routes. De Smith (2004) shows that Distance Transforms (DTs) can be modified and used to solve optimization problems involving location theory, path determination, planning and decision support. Distance transforms can be combined and weighted to generate alternatives which can be used to solve problems in spatial decision making. These weighted distance transforms are referred to as multiple weighted distance transforms (MWDT). Another modification is the variable topography distance transforms (VTDTs) which allows determination of shortest paths across physical landscapes. This can be used to optimize the route

selection and placement of separators and power plants. The third extension to distance transforms introduces cost dimension. Under certain circumstances, shorter routes may be more expensive. Also the route may cause a longer travelling time to reach a point of interest due to certain challenges. To address this problem distance transforms can be modified to capture such interests and are referred to as least cost distance transforms (LCDT).

2.3.1 Separator and power plant placement

The location of a separator is always a very challenging exercise for steam field designers. The argument is whether to locate satellite separators close to well heads with longer steam pipelines running to power stations or have them centralized for many wells and close to the power station. Many authors have researched and written about this subject. Satellite separators located close to well heads will result in good scrubbing of solid minerals from separator carry over as well as good moisture removal of condensates through drain pots along the long pipeline (Lee, 1982). It will also reduce the need for using large scrubbers and steam demisters or vortex separators (Lee, 1995) near the power stations. On the other hand, centralized separators located close to the power station will result in shorter steam pipelines to the power station that are easy to control, have lower pressure drop and are cheaper. However, it is necessary to have large scrubbers and demisters near the power stations to improve the purity and quality of the steam entering the turbine. Entry of steam condensate to the turbine can also be minimized by having the power station at higher elevation than the steam field. According to Watson et al. (1996), separator location should be chosen in a way that it prevents flashing in the separated water (brine) pipelines.

The location of a separator needs to balance all the conditions and is an optimization problem. From experience in the Olkaria field (author's experience), optimal separator location tends to be central one where a separator can handle a group of wells from either the same pad or from different pads. For this study, the optimal separator location is obtained using weighted distances in the VTDT algorithm. Topology considerations and design restrictions are also considered. In the event of individual wells which are found to be inappropriately situated from the optimal location, consideration should be made for placement of individual separator in an appropriate location.

Power plant placement is done taking into account separator stations, the environmental issues, accessibility and operational issues. It is important for instance to locate the power plant in such a way that entry of steam condensate to the turbine is avoided. This may be achieved by locating the plant in higher elevation compared to supply steam lines from separator stations. In the distance transform algorithm, this is achieved by imposing a gradient constraint between delivery lines and desired location.

2.4 Cost issues in geothermal steam system

The cost of geothermal steam system development consisting of piping costs and separator costs is a critical component of the overall cost of geothermal projects. Several estimates have been put forward to quantify the actual value with regard to the total cost of the project. Oyango (2015) reports that the steam gathering system contributes about 10% of the overall cost of the geothermal field development. However, the process of cost determination is a highly secretive venture as information required is often held classified by the suppliers for competitional reasons.

The main components of cost in a steam system are piping and separator material cost, installation cost, cost of fittings, welding costs, bends and bend installation cost. The cost of access roads and civil works can be treated separately under infrastructure costs. The piping installation cost is made up of material (30%), fittings (10%), installation labour (25%), installation equipment (10%), supports (15%) and P&G (10%). The total cost can vary from US$ 600 to US$ 1200 per meter, depending on pipe diameter, slope of the terrain, cross-country or well pad piping (Henriquez and Aguirre, 2011).

In this report, the piping and separator material cost is evaluated as it forms the bulk of the steam system cost. Depending on the temperature of the fluid both metallic and non-metallic piping can be used in geothermal application. Steel is the most widely used material due to its ability to handle high temperatures and longer service life. Thus, the cost of steel greatly influences the cost of the pipes. Similarly, the costs for equipment, installation, bending and bend installation and welding increase with increasing pipe nominal diameter (Kalinci et al., 2008).

3. METHODOLOGY

This chapter describes the procedure carried out in this study. It involves determination of optimum location for separator station with respect to production wells, hot reinjection wells and the power plant. The first step is to optimize the location of separator stations and the second step involves optimal placement of the power plant with respect to optimized separator locations. Each optimization step also defines the route and total distance of the route. The study employs the use of distance transforms to determine the path to the proposed optimal locations, specifically a modified form of distance transform, which involves weighting of variable topography distance transform (VTDT) to become weighted variable topography distance transform (WVTDT).

3.1 Distance transforms (DTs)

The central function in the distance transform algorithm is given by the Bellman's Equation 1 expressed as (de Smith, 2004):

$$d_{i,j} = min(d_{i+m,j+n} + c_{m,n}, d_{i,j}) \quad (1)$$

where $d_{i,j}$ is the value of the distance matrix at the central point of the chamfer mask, $d_{i+m,j+n}$ is the value of the distance matrix at the same location from the central point as $c_{m,n}$ is placed in the chamfer matrix. The algorithm involved is in the order of Mn^2 computations where n is the maximum dimension of the lattice, and M is the number of cells used in the neighbourhood computation.

In the above distance transform algorithm, the objective function works with a two-pass scan (forward and backward) of a square or rectangular lattice data set. Each pass involves adding values in a divide form of the adjacency matrix or mask to cell in the underlying lattice as shown in Figure 3. The value in mask position of the transformed lattice is then set to the minimum of the calculated sums.

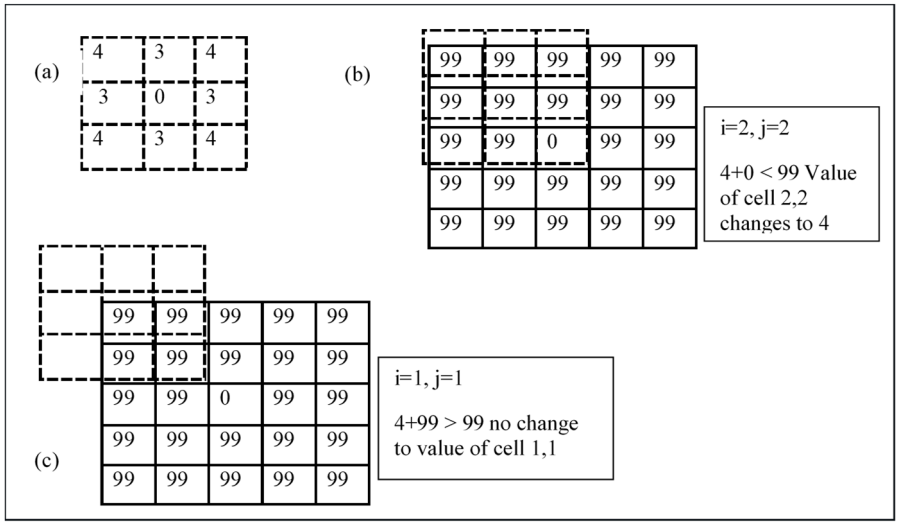

FIGURE 3: (a) 3 x 3 integer chamfer masks for distance transformation; (b) and (c) are forward scans (Jónsson, 2016a)

3.1.1 Variable topography distance transform (VTDT)

The variable topography distance transform (VTDT) works with the digital elevation matrix (DEM). Basically, DEM is a digital representation of real-world ground topography where the rectangular lattice

of points or cells has allocated elevation values. VTDT is a chamfer distance metric with each point having latitude, longitude and altitude (height) values assigned. In this case therefore, the chamfer matrix and distance transform is extended to a 3D model. The value in the cell represents the elevation value at that particular point, hence, given two points the gradient can be evaluated. In route selection therefore, the gradient phenomenon is added to the distance transform algorithm as a constraint. The resultant function is a modified function incorporating the gradient given by Equation 2:

$$\begin{gathered} if\ \{([d_{i+m,j+n}\ + c_{m,n}] <\ d_{i,j})\ and\ (\left|S\right| < Smax)\} \\ then\ \ d_{i+m,j+n}\ + c_{m,n} \end{gathered} \tag{2}$$

where maximum allowable slope, ($Smax$), is the constraint value and slope (S) is the magnitude of the path gradient.

This function is referred to as the gradient constrained transform (GCDT) and can be applied to other target points or lines like existing roads for exclusion in the route design. Solving the equation by iteration of the GCDT scanning algorithm results in optimal paths selected with small differences in the total surface path length. However, by modification of the maximum gradient constraint over a range of values above or below the target, it is possible to determine a series of solution paths with further iterations.

The solutions of the path lengths obtained can further be subjected to a cost constrained. If a generalized cost field is introduced and can be defined over the rows (r) and columns (c) of the lattice as COST (r, c), then the central distance transform function can be modified to incorporate cost as in Equation 3:

$$d_{i,j} = \min\ (d_{i+m,j+n}\ + c_{m,n}\text{*[COST(r, c)], } d_{i,j}) \tag{3}$$

By evaluating the equation above for every alternative path, one can compare the cost of each path and the optimal path is the one with minimum cost.

3.1.2 Multiple weighted distance transforms (MWDT)

As MWDT involves alternative routes, the general equation involves obtaining a weighted sum z of multiple transforms. If we denote distance transform of type k applied to an object set $\{A_i\}$ as $DT_k\{\mathrm{A_i}\}$, then the weighted sum of MWDT can be deduced from Equation 4 as:

$$z = \sum_i w_i\, DT_k\{A_i\} \tag{4}$$

This is a composite surface or set of values with one or more minima. In this kind of problem, it is possible to find one point that can minimize the sum of the distances as a function of each of the vertices. According to de Smith (2004), MWDT fails to accurately locate the point. The introduction of WVTDT in this project addresses the shortcoming in MWDT.

3.2 Route selection, separator and power plant placement and optimization

The aim of route selection is to identify the shortest path that avoids restricted areas like park reserve sites, unnecessary crossing of roads and rivers and excessively steep slopes which would make construction work difficult or push costs up. Generally, this includes consideration of environmental effects and public safety. In this study, variable topography transform (VTDT) is used to find the shortest distance.

A 2-D matrix is used in the DEM model, where every element $(H_{i,j})$ represents the height of allocation on the surface with coordinates *(i,j)*. The slope is then calculated from the altitudes of the cells obtained from the DEM and a maximum gradient constraint (S_max) is applied. The normal distance transform equation is modified to Equation 5:

$$S = \frac{(H_{i+m,j+n} - H_{i,j})}{c_{m,n}} \tag{5}$$

Hence if the slope is *S* and maximum allowable slope is *Smax,* then:

$$\begin{gathered} if\left(d_{i+m,j+n} + c_{m,n} < d_{i,j}\ and\ S < Smax\right); \\ \text{then } d_{i,j} = d_{i+m,j+n} + c_{m,n} \end{gathered} \tag{6}$$

If Equation 6 returns untrue, no route can lie between the two cells in question. The equation therefore ensures that the gradient of the "shortest route" is within the desired value, whereby the gradient constraint is implemented in the condition in Equation 7 and 8:

$$\begin{gathered} If\ \ (H_{i+m,j+n} - H_{i,j} < \Delta H_c\ and\ S_{i+m,j+n} < S_c) \\ then\ \ d_{i,j} = \min\left(d_{i+m,j+n} + c_{m,n}, d_{ij}\right);\ else\ d_{i,j} = d_{i,j} \end{gathered} \tag{7}$$

where $H_{i+m,j+n}$ and $S_{i+m,j+n}$ are height and slope respectively, both calculated from the altitudes of the particular cells from the DEM. The constraints, critical height ΔH_c and critical slope S_c, are user defined.

The way to define the critical values was proposed by Kristinsson (2005), where the altitude values of the cells representing constraints are set to either Not a Number (NaN) or a very high number. In this case, the excessively high resultant gradients will fail the maximum height test.

3.3 Topology design and pipeline design criteria

The standard pipeline design process involves (Jónsson, 2016b):

1. Topology and route selection;
2. Demand and flow analysis;
3. Pipe diameter optimization (minimum cost due to head loss);
4. Thickness and pressure class design;
5. Thermal stress analysis (anchors, expansion loops and expansion units); and
6. Pump sizing and arrangement.

However, this study is limited to pipe diameter optimization and thickness and pressure class designs. The topology design optimizes the distances between the production wells and separator stations and from the separator stations to the re-injection wells and the power plant. This is done by organizing the output from the distance transform in the route selection above into a distance table. Flow in the different pipeline options can be optimized in excel using the Solver ad-in program.

3.4 Pipe diameter optimization

The selection of the correct pipe diameter is very important in hydraulic calculation as this would ensure smooth flow of fluid which can be devoid during pulsing operation of the pipeline. The pipe diameter also has a critical influence on pressure drop in the pipeline together with other parameters like bends or irregularities in the pipe layout. It is also necessary to have pipe thicknesses of the right structural

strength that can withstand pressure as well as other external loads like wind and earthquakes. The main optimization goal is to minimize cost and reach acceptable pressure drop along the pipeline. Optimization of pipe diameters for brine flow, steam flow and two-phase flow is done separately due to different conditions in the different fluid pipelines. The process is done by considering single-phase flows first, then the two-phase flow.

3.5 Single-phase pressure drop

This is where the fluid in the pipe is in one phase, either liquid or steam. In this study the brine leaving the separator to the turbine is saturated. Similarly, the brine coming from the turbine for reinjection is saturated. Generally, the primary variables in single-phase flow are velocity, pressure, enthalpy and density.

Single-phase pressure drop is calculated from the Darcy-Weisbach Equation (Equation 8). The two main controlling pressure drops are the frictional and static pressure drops. Friction pressure loss is influenced by fluid velocity, pipe internal diameter, pipe roughness and Reynolds number while the static loss is basically the difference in elevation between the start and end of the pipe.

$$\frac{dp}{L} = f\frac{\rho v^2}{2D_i} \tag{8}$$

where dp is the pressure drop (Pa), L the length of pipe (m), f the friction factor, ρ fluid density (kg/m^3), v flow velocity (m/s) and D_i the internal pipe diameter (m).

The pressure drop can also be rewritten in terms of head loss (dh) given by Equations 9 and 10:

$$dp = \rho\, g\, dh \tag{9}$$

Hence,

$$\frac{dh}{L} = f\frac{v^2}{2gD_i} \tag{10}$$

The Reynolds number Re is then calculated using Equation 11 below:

$$Re = \frac{\rho v D_i}{\mu} \tag{11}$$

where μ is the dynamic viscosity of the fluid in SI units (Pa s).

The Colebrook-White equation (approximated in Equation 12) is then used to calculate the friction factor, f:

$$f = \frac{0.25}{\left(log_{10}\left(\frac{\epsilon}{3.7\,D_i} + \frac{5.74}{Re^{0.5}}\right)\right)^2} \tag{12}$$

where ϵ is the pipe roughness. The Moody diagram can also be used to approximate the friction factor.

3.6 Two-phase flow pressure drop models

Two-phase flow involves flow of both steam and water in the same pipe at same time. However, in geothermal fluid flow, there exist non-condensable gases in the mix but this is usually a very small proportion of the total flow hence disregarded in calculations. Two-phase flows can be classified into

different flow regimes using flow regime maps. Some regimes like slug and plug are not desirable as they often lead to damage of pipelines resulting in high maintenance costs. The selection of optimum diameter for a two-phase flow pipe aims to avoid such regimes. Two critical parameters involved are reasonable pressure drop and maximum steam velocity which is recommended to be at a range of 25 to 40 m/s. Generally, a smaller diameter is preferred due to cost but pressure drop must be within acceptable limits.

There exist many models that have been used to predict the pressure drop in two-phase flow. In broad terms they are commonly classified as homogenous flow models and separated flow models (Pálsson et al., 2006).

3.6.1 Pressure drop in homogenous flow model

In homogeneous flow, the two phases are treated as a single fluid, with the two phases uniformly distributed over the flow cross-section area with the same flow direction and velocity. The thermodynamic and hydrodynamic properties can therefore be assumed to be defined by the mean values of properties of the two phases. The homogeneous void fraction derived from averaging the properties of the two phases is used. The void fraction is the term used for the ratio of area occupied by the steam to the pipe cross-sectional area. The total pressure drop in a homogeneous flow model is given by the sum of static pressure drop (elevation head), momentum pressure drop (acceleration), and frictional pressure drop (h_f). The homogeneous flow void faction (ε), which is given by Equation 13, can be used to estimate the cross-sectional areas occupied by the gas and the liquid phases:

$$\alpha = \frac{1}{1 + \left(\frac{1-x}{x}\right) * \frac{\rho_g}{\rho_l}} \tag{13}$$

The other critical parameters in the estimation of friction pressure drop, $dp_{friction}$, are two-phase viscosity, homogeneous density, homogenous Reynolds number and two-phase friction factor which are calculated using the respective equations below. Two-phase viscosity is calculated by Equation 14:

$$\mu_{tp} = x\mu_g + (1-x)\,\mu_l \tag{14}$$

where x is the quality (the gas mass flow fraction).

Homogenous Reynolds number and homogeneous density are given by Equation 15 and 16, respectively:

$$Re = \frac{D_{in} * \dot{m}_{total}}{\mu_{tp}} \tag{15}$$

$$\rho_{tp} = \alpha\rho_g + (1-\alpha)\rho_l \tag{16}$$

where α is the area averaged local void fraction of the gas, ρ_g and ρ_l are the densities of the gas and the liquid.

Two-phase friction factor for homogenous flow is given by Equation 17:

$$f = \frac{0.079}{Re^{0.25}} \tag{17}$$

Hence, the homogenous friction pressure drop can be calculated by optimizing the inner pipe diameter by restricting the velocity of the two phases to 40 m/s. Equation 18 thus applies:

$$\Delta\, p_{friction} = \frac{2f\dot{m}^2{}_{total}}{d_{in}\rho_{tp}} \tag{18}$$

The momentum pressure gradient per unit length for homogenous flow is given by Equation 19:

$$(\frac{dp}{dz})_{momentum} = d\frac{\left(\frac{\dot{m}_{total}}{\rho_{tp}}\right)}{dz} \quad (19)$$

The static pressure drop is given by Equation 20:

$$\Delta p_{static} = \rho_{tp}\, g\, \Delta H \quad (20)$$

The total two-phase pressure drop for homogenous model in this study considered the static and friction pressure drop calculated from Equation 21:

$$\Delta p_{total} = \Delta p_{static} + \Delta p_{friction} \quad (21)$$

3.6.2 Pressure drop in separated flow models

Separated flow models assume that the gas and the liquid phases flow separately with distinct mean properties for each phase. Interactions within the phases, between the phases, and between phases and channel walls are evaluated separately in order to find a suitable correlation for predicting pressure drop.

Separated flow model mimics two distinct pipelines each carrying the equivalent of a single-phase fluid with each fluid occupying a certain percentage of the cross-sectional area in the pipeline and having distinct mean properties for each phase. To estimate the pressure drop in separated flow, knowledge of the void fraction is a mandatory requirement. The total pressure drop is the sum of four different pressure loss terms for each fluid which are friction, dynamic, acceleration and elevation pressure losses. Correlations describing pressure drop in two-phase flow revolve around two main approaches: conservation of momentum and conservation of energy. Several correlations have been developed for calculating void fraction in separated flows and can be classified as either analytical or empirical models

a) Analytical void fraction models
In this category, the Zivi kinetic energy model for annular flow and the Levi momentum model are mostly used. Zivi derived two models, one for liquid entrainment in gas phase and the other assumes no liquid entrainment in the gas phase. The Levi correlation on the other hand assumes that momentum is exchanged constantly between the two phases as the fluid properties vary and the flow tends to maintain a value which is equal to the sum of frictional and static head losses in each phase. Neither correlation is used in this study.

b) Empirical void fraction models
Several empirical correlations for void fraction exist together with recommendations on how to apply for best results. In this section, some of the most recommended are described.

Harrison (1975) correlation method
This correlation is derived from the analysis of two-phase flow velocity distribution using the Seventh Power Law which is given in Equation 22:

$$\frac{1-\alpha}{\alpha^{7/8}} = \left[\left(\frac{1-x}{x}\right)\left(\frac{\rho_g}{\rho_l}\right)(\frac{\mu_l}{\mu_g})\right]^{7/8} \quad (22)$$

This method is recommended for large diameter pipes (Zhao et al., 2000). The gaseous-phase volume flow rate $\dot{v}_g$ from the seventh power law is applied to two-phase flow velocity distribution that results in Equation 23:

$$\dot{v}_g = \frac{49}{60}\, U_g \pi\, R^2 \alpha \quad (23)$$

where U_g is the gaseous phase centreline velocity.

And the gaseous mass flow rate $\dot{m}_g$ is calculated from Equation 24:

$$\dot{m}_g = \frac{49}{60}\,\rho_g\,U_g\pi\,R^2\alpha \tag{24}$$

The velocity distribution for the gaseous phase is given by Equation 25:

$$\overline{u} = \overline{u_{ip}} + U_g\left(1 - \frac{r}{\sqrt{\alpha}R}\right)^{\frac{1}{7}} \tag{25}$$

where $\overline{u}$ is velocity at radius r, $\overline{u_{ip}}$ is the interphase velocity, U_g is the gaseous-phase centre velocity and R is the pipe radius.

Similarly for the liquid phase, the seventh power law yields the following Equations 26 and 27 for liquid volume flow rate ($\dot{v}_f$) and liquid mass flow rate ($\dot{m}_f$) respectively:

$$\dot{v}_f = \frac{49}{60}\,U_f\pi\,R^2\left(1-\sqrt{\alpha}\right)^{\frac{8}{7}}\left(1+\frac{8}{7}\sqrt{\alpha}\right) \tag{26}$$

$$\dot{m}_f = \rho_f\ v_f \tag{27}$$

Now the average liquid-phase film velocity is calculated from Equation 28:

$$\overline{v_f} = \frac{\dot{v}_f}{A_f} = \frac{49}{60}U_f\frac{(1-\sqrt{\alpha})^{\frac{8}{7}}\,(1+\frac{8}{7}\,\sqrt{\alpha})}{(1-\alpha)} \tag{28}$$

while the average velocity of the equivalent single-phase flow is defined by Equation 29:

$$\overline{v_{eq}} = \frac{\int_0^R U_f\,(1-\frac{r}{R})^{1/7}\,2\pi r dr}{\pi R^2} = \frac{49}{60}U_f \tag{29}$$

Velocity ratio ($\frac{\overline{v_f}}{\overline{v_{eq}}}$) is used in predicting pressure drop and is calculated from Equation 30:

$$\frac{\overline{v_f}}{\overline{v_{eq}}} = \frac{(1-\sqrt{\alpha})^{\frac{8}{7}}\,(1+\frac{8}{7}\,\sqrt{\alpha})}{(1-\alpha)} \tag{30}$$

Lockhart Martinelli correlation

The Lockhart-Martinelli correlation makes use of the friction multiplier (also known as two-phase multiplier) approach for predicting two-phase pressure drop. This approach relates the two-phase frictional pressure gradient in terms of frictional multipliers both for gas ($\emptyset^2{}_g$) and for liquid ($\emptyset^2{}_l$) which are assumed to flow independently inside the pipe. The two multipliers for gas and liquid are defined in Equations 32 and 33, respectively, as:

$$\emptyset^2{}_g = \frac{\left(\frac{dp}{dz}\right)_{ftp}}{\left(\frac{dp}{dz}\right)_{fg}} \tag{32}$$

$$\emptyset^2{}_l = \frac{\left(\frac{dp}{dz}\right)_{ftp}}{\left(\frac{dp}{dz}\right)_{fl}} \tag{33}$$

where $\left(\frac{dp}{dz}\right)_{ftp}$ is the two-phase pressure gradient and $\left(\frac{dp}{dz}\right)_{fg}$ and $\left(\frac{dp}{dz}\right)_{fl}$ are the pressure gradients for gaseous phase and liquid phase flowing alone in the pipe.

Then Lockhart-Martinelli parameter or pressure drop ratio (X) is defined as given by Equation 33:

$$X^2 = \frac{\left(\frac{dp}{dz}\right)_{fl}}{\left(\frac{dp}{dz}\right)_{fg}} = \left(\frac{1-x}{x}\right)^{1.8}\left(\frac{\rho_g}{\rho_l}\right)\left(\frac{\mu_l}{\mu_g}\right)^{0.2} \tag{33}$$

By relating the two-phase frictional pressure gradient to the gradient for the steam phase, the single-phase pressure drop for steam can be calculated from the standard Equation 34 below:

$$\left(\frac{dp}{dz}\right)_{fg} = f\left(\frac{L}{D}\right)\frac{1}{2}\,\rho_g {V_g}^2 \tag{34}$$

Consequently, the two-phase pressure drop can be derived using Equation 35:

$$\left(\frac{dp}{dz}\right)_{fTP} = \phi^2 f\left(\frac{L}{D}\right)\frac{1}{2}\,\rho_G {V_G}^2 \tag{35}$$

where dp is the two-phase pressure drop (N/m^2) while ϕ^2 is the two-phase multiplier (dimensionless), f is the friction coefficient, L the effective length, D is the inside diameter of pipe, while ρ_g is the density of steam (kg/m^2) and ${V_g}^2$ is the velocity of steam if it was flowing alone in the pipe (m/s).

The velocity of steam can be found from Equation 36:

$$V_g = \frac{4\,m\,x}{\rho_g \pi D^2} \tag{36}$$

Hence, the two-phase pressure drop due to friction can be calculated using Equation 37:

$$\Delta p = \frac{8}{\pi^2}\phi^2\,\frac{L\,f\,(m\,x)}{D^5 \rho_g} \tag{37}$$

The friction coefficient *f* is a function of Reynolds number Re and pipe wall roughness factor is ϵ . The Reynolds number of the steam phase is given by Equation 38:

$$R_{e\,g} = \frac{\rho_g\,V_g D}{\mu_g} \tag{38}$$

where μ_g is the dynamic viscoity for the steam phase (kg/ms). The friction coefficient *f* for rough pipes is calculated from the Colebrook and White relation (Equation 39).

$$f = 1.74 - 2\log\left(\frac{2\epsilon}{D} + \frac{18.7}{R_e\sqrt{f}}\right) \tag{39}$$

However, for $R_e > 4{\cdot}10^4$ the friction factor can be approximated by Equation 13 (Jónsson, 2016b).

Friedel correlation

The Friedel correlation relates the two-phase frictional pressure gradient to the frictional pressure gradient for a single-phase flow at the same total mass velocity but with the physical properties of the liquid phase, namely $\left(\frac{dp}{dz}\right)_{flo}$. In this case, the two-phase frictional multiplier ϕ is defined by Equation 40:

$$\phi_{lo}{}^2 = \frac{\left(\frac{dp}{dz}\right)_{ftp}}{\left(\frac{dp}{dz}\right)_{flo}} \tag{40}$$

The Friedel correlation for the vertical upward flow and horizontal flow is defined as Equation 41:

$$\phi_{lo}{}^2 = E + \frac{(3.24FH)}{Fr^{0.045}We^{0.035}} \tag{41}$$

where the Froude number Fr, Weber number We, and parameters H, E and F are defined by Equations 42-46, respectively:

$$Fr = \frac{m^2}{gD\rho_{tp}{}^2} \tag{42}$$

$$We = \frac{m^2 D}{\rho_{tp}\sigma} \tag{43}$$

$$H = \left(\frac{\rho_l}{\rho_g}\right)^{0.91}\left(\frac{\mu_g}{\mu_l}\right)^{0.19}\left(1 - \frac{\mu_g}{\mu_l}\right)^{0.7} \tag{44}$$

$$E = (1-x)^2 + x^2\left(\frac{\rho_l f_{go}}{\rho_g f_{lo}}\right) \tag{45}$$

$$F = x^{0.78}(1-x)^{0.24} \tag{46}$$

In the above set of equations, μ_l is the dynamic viscosity for liquid measured in kg/ms, σ is the surface tension in N/m while f_{go} and f_{lo} are the friction factors calculated as if the liquid and the gas respectively were flowing alone in the pipe.

For this particular correlation, ρ_{tp} is given by Equation 47:

$$\rho_{tp} = \left[\frac{x}{\rho_g} + \frac{(1-x)}{\rho_l}\right]^{-1} \tag{47}$$

According to Hewitt (1982), the following recommendations are made for use with the above correlations:

I. For $\frac{\mu_l}{\mu_g} < 1000$, the Friedel correlation should be used;
II. For $\frac{\mu_l}{\mu_g} > 1000$, and $m > 100$, the Chisholm correlation (Hewitt, 1982) should be used; and
III. For $\frac{\mu_l}{\mu_g} > 1000$, and $m < 100$, the Martinelli correlation should be used.

c) Pressure drop in bends

Calculation of pressure drop in bends and fittings is done by using the equivalent length technique. Ouma (1992) reports that increasing the pipe length by 15% can compensate for pressure losses in bends and fittings. Since this study has same pipeline properties as the one in Ouma's case, similar assumption would be made.

3.7 Pipe thickness, pressure class and mechanical stress analysis

3.7.1 Pipe thickness and pressure class

The structural analysis of the pipes takes into consideration the design code ASME B31.1 (ASME, 2007) which outlines the equations for pipe stress analysis. The wall thickness T_m is determined by Equation 48:

$$T_m = \frac{pD_o}{2(SE + Py)} + A \tag{48}$$

where T_m is wall thickness (mm), p is the design pressure (kPa), the pipe outside diameter D_o is given in millimetres, *SE* is the allowable stress (kPa), *y* is a constant based on temperature range and steel type and *A* is the corrosion and erosion allowance. In most geothermal applications *y* is 0.4 while *A* is 3 mm.

The operating pressure for individual wells has to be optimized to result in maximum flow. However, when wells in the same fields have different well head pressure, it is difficult to optimize. In this case, the design pressure is set by considering the highest pressure of the wells in question and adding a margin of safety.

3.7.2 Mechanical stress analysis, bending moments and length of supports

According to Henriquez and Aguirre (2011), stress analysis should be carried out for the following load cases in piping design: sustained loads, occasional loads, operational loads and thermal loads. Also bending moments and pipe support designs have to be investigated, this is however not included in the scope of this report

3.8 Separator dimensional design and cost estimation

The separator considered is the vertical cyclone separator which is the most common in the Olkaria field. The separator works more or less as a centrifuge that creates a vortex that pushes the heavier liquid phase to the walls of the vessel while the lighter gaseous phase remains in the middle. The liquid will move down along the walls of the vessel and is collected at the bottom while the lighter steam will move up and will be directed into the centrally placed delivery tube downwards to leave the vessel through the bottom pipe as shown in Figure 4. The critical parameters controlling the size of the separator are separation pressure, flow enthalpy and total mass flow in the separator.

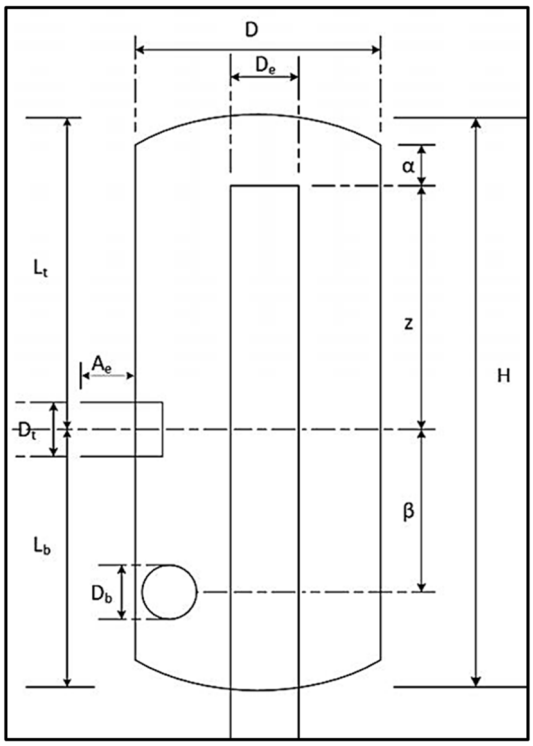

FIGURE 4: Vertical cyclone separator

The first step in designing the separator is to determine the terminal velocity v_t as a function of liquid density ρ_l and vapour density ρ_g. Equation 49 below defines this relationship:

$$v_t = K' \left[\frac{\rho_l - \rho_g}{\rho_g}\right]^{1/2} \tag{49}$$

where K' is a constant based on gravity, droplet diameter and drag coefficient of a liquid particle.

For most systems, the constant K' ranges between 0.012 and 0.030, however a recommended value of 0.069 m/s is to be used except where special considerations are required (Gerunda, 1981).

The inlet size pipe diameter D_t, is calculated from the relationship given below in Equation 50:

$$D_t = \left[\frac{4A_i}{\pi}\right]^{1/2} \tag{50}$$

where A_i is the cross-sectional area of inlet pipe expressed in terms of volumetric steam flow.

Q_{vg}, is given in Equation 51:

$$A_i = \frac{Q_{vg}}{v_t} \tag{51}$$

The general guidelines recommended for cyclone separator design are summarised in Table 1 (DiPippo, 2007).

TABLE 1: Cyclone separator design guideline (DiPippo, 2007)

Parameter	Separator speed
Maximum steam velocity at 2-phase inlet pipe	45 m/s
Recommended range of steam velocity at 2-phase inlet pipe	25 - 40 m/s
Maximum upward steam velocity inside separator	4.5 m/s
Recommended range of upward annular steam velocity inside cyclone separator	2.5 - 4.0 m/s

Several studies have been done on separator dimensions determination. In this study approaches by Bangma (1961) and Lazalde-Crabtree (1984), together with the spiral inlet guidelines for separator sizing proposed by Purnanto et al. (2012), as shown in Table 2 below, will be considered. All three approaches determine the various dimensions of the separator as a function of separator inlet pipe diameter.

The thickness of the separator will be determined in the same way as pipe wall thickness to satisfy the condition that it should be sufficient to withstand the pressure of the separator in working condition. The pipe thickness (Equation 48) as per ASME shall apply. The performance of the separator is measured by comparing the proportion of brine to the mass flow rate of water entering the separator. This ratio gives the separator efficiency. Field experience with operation of separators indicates that 100% efficiency is not practical. Typical separator efficiencies of between 99.5% and 99.9% have been reported by some studies (Onyango, 2015). However, efficiency measurement is out of the scope of this report.

TABLE 2: Vertical separator design guidelines
(Purnanto et al., 2012)

Parameter	Bangma design	Lazalde-Crabtree design	Spiral-inlet design
D	$3D_t$	$3.3D_t$	$2.95D_t$
D_e	$0.8D_t$	$1D_t$	$1D_t$
D_b	$1D_t$	$1D_t$	$0.7D_t$
α	$3.25D_t$	$0.15D_t$	$0.28D_t$
β	$3D_t$	$3.5D_t$	$3.2D_t$
Z	$3D_t$	$5.5D_t$	$5.8D_t$
L_T	$7D_t$	$6.475D_t$	$6.8D_t$
L_B	$4.5D_t$	$4.975D_t$	$4.9D_t$

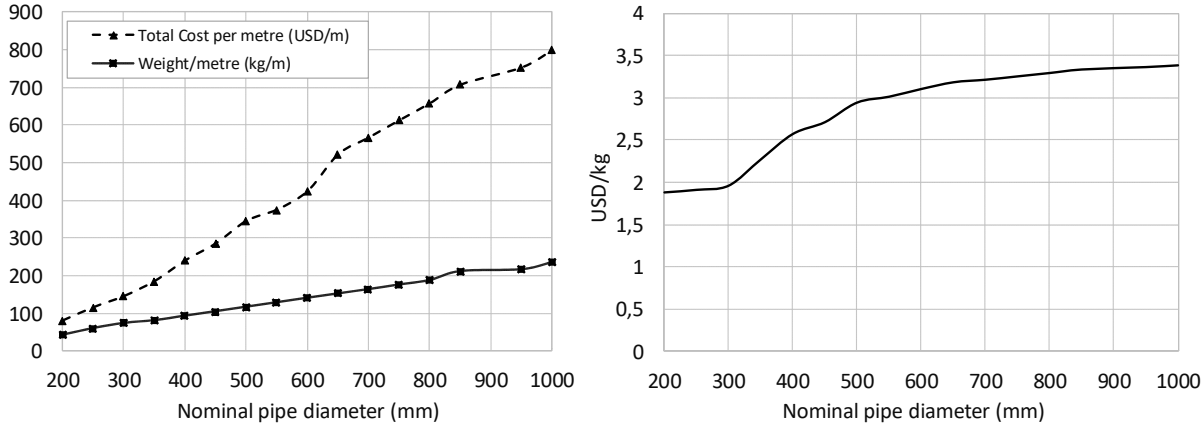

FIGURE 5: Graphs of a) Nominal pipe diameter vs cost per metre and weight per metre; and b) Nominal pipe diameter vs cost per kilogram

3.8.1 Cost estimation

Pipes are manufactured in different grades and schedules depending on the application, and prices will therefore vary from one grade to another and between schedules and diameter sizes. Separators on the other hand are non-standard equipment which are produced according to the client requirements and application. A good way of estimating a generalized initial cost of such equipment will be to find the total weight of material required to make the equipment and then determine cost of material per unit weight. This procedure is used in this study. The cost values used are derived from cost variation values presented by Kalinci et al. (2008) and summarized in Table 3 below. Using Excel, the values are interpolated to cover pipe diameters not included in Kalinci's report.

TABLE 3: Values of different cost elements for different nominal pipe diameter (Kalinci, 2008)

Nominal pipe diameter	Total cost per metre (USD/m)	Pipe installation cost (USD/m)	Pipe bend cost (USD/bend)	Bend installation cost (USD/m)
0.20	50	30	150	25
0.25	70	45	300	50
0.30	90	55	450	100
0.35	115	79	700	225
0.40	150	90	950	275
0.45	175	110	1350	375
0.50	215	130	1750	403

A graph of nominal diameter as a function of each of the cost elements and the total pipe cost is illustrated in Figure 5. The cost of pipe per unit weight for each pipe nominal diameter can be evaluated. The values for the data provided in the report by Kalinci et al. (2008) and after interpolation is presented in Table 4 below.

The cost of steel material per metre is evaluated by comparing total cost per metre from Kalinci (2008) data and the pipe chart from Tiago pipe supplies (Tioga, 2014), which is given in Appendix I per metre of steel pipe for different pipe diameters.

TABLE 4: Variation of pipe cost per kilogram with nominal diameter

Nominal pipe diameter (mm)	Total cost per length (USD/m)	Weight per length (kg/m)	Cost per weight (USD/kg)
0.20	80.0	42.5	1.88
0.25	115.0	60.29	1.91
0.30	145.0	73.86	1.96
0.35	185.0	81.33	2.27
0.40	240.0	93.27	2.57
0.45	285.0	105.17	2.71
0.50	345.0	117.15	2.94
0.55	374.9	129.14	3.01
0.60	424.4	141.12	3.10
0.65	522.1	152.88	3.18
0.70	567.0	164.40	3.21
0.75	613.1	176.68	3.25
0.80	658.1	188.83	3.29
0.85	707.7	212.57	3.33
0.95	753.6	217.57	3.36
1.00	799.4	236.62	3.38

4. RESULTS AND DISCUSSIONS - CASE STUDY OLKARIA IV FIELD

4.1 Field data

Appendix II shows some properties of the wells in the Olkaria IV field serving separator SD2 while Table 5 contains details of all four separators in the field.

TABLE 5: Olkaria IV field separators data

Separator	Northing (m)	Easting (m)	Elevation (m)	Separator capacity (MW)	Steam flow (kg/s)
SD1	202340	9899980	1985	24.2	36.4
SD2	203160	9900630	1960.4	8.0	134.7
SD3	203650	9898900	2010	74.0	124.2
SD4	204510	9899170	2029	67.7	12.5

In the current status, separator station SD2 has three separators SD2A, SD2B and SD2C. The test data for wells serving each separator are presented in Table 6.

Some observations and assumptions made in the process of this study include:

1. The well parameters are used as per results of well test data and separation pressure is predetermined.
2. Separation pressures for all separators are predetermined as 12 bars.
3. For separator placement exercise, only separator SD2 will be considered for optimization illustration and new coordinates obtained. An assumption is made for the remaining three, current locations are used as optimized locations.
4. Power plant placement will be done taking into account all the separators. In this case, distances from production and reinjection wells have been taken care of during separator placement. The cold reinjection wells are not considered since they are made of low budget plastic (HDPE) making its cost negligible compared to the price of steel piping for the other pipelines.

TABLE 6: Olkaria IV SD2 separator station well test data

Separator	Wells	Well head pressure	Separator pressure	Two-phase mass flow (t/h)	Enthalpy (kJ/kg)	Steam flow (t/h)	Steam flow (kg/s)	Brine flow- (t/h)	Power (MWe)
SD2A	908	14.9	12	30	2200	21.2	5.9	8.8	4.0
	908A	17.5	12	115	14200	36.1	10.0	78.9	6.0
	908B	14.7	12	87	2050	54.9	15.3	32.1	8.8
	910	18.3	12	60	1950	34.8	9.7	25.2	4.6
						(147)		(145)	
SD2B	910A	18.1	12	110	2250	80.5	22.4	29.5	13.0
	910B	18.6	12	210	2000	127.3	35.4	82.7	14.9
						(207.8)		(112.2)	
SD2C	909	12.9	12	130	2000	78.8	15.3	51.2	12.5
	909A	12.4	12	100	1820	51.5		48.5	10.2
						(130.3)		(99.7)	
Total				842		485	134.7	357	74.0
Average			12		1941				

5. The steel prices used are estimates from previous studies and not actual prices.
6. SI units are used in all calculations.
7. For the pipeline cost, only the cost of material and installation are considered.
8. Upward flow for the two-phase flow is restricted to a specified slope for each case.

4.2 Route selection and separator SD2 placement

In this study, coordinates of the point that is optimized (separator location) is treated as a sample point identified as separators, while the well coordinates are defined as endpoints.

This is a two-step process. The first step is to find the best place to locate the separator with respect to all production wells leading to it, all hot reinjection wells from the separator and the power plant. The reference point of interest (separator) is a sample (S) point while all wells (production and hot reinjection) and power plant are endpoints (E). The coordinates of the sample and end points are inputs to the VTDISTRA program. The constraints included are maximum height difference, maximum slope and route weight as indicated in sample input file (Appendix III). The output results of the program include a digital elevation map (Figure 6), distance maps and weighted distance maps of the area in question showing positions of all input points and relative distances from the initial location of the separator. The routes and distances from each end point to the current location of the separator is shown in the maps and the best location of the separator is given. An output file shown in Appendix IV also captures the coordinates of the optimized separator location, total distance to each end point and coordinates of the route sampled with one metre intervals.

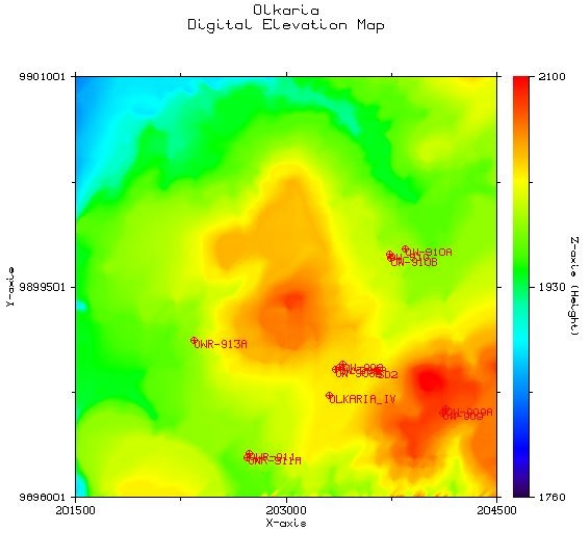

FIGURE 6: Olkaria IV distance map

The second step utilises the new optimized separator coordinates as sample point and a second run gives optimized distances of all end points to the optimized location of the separator. Depending

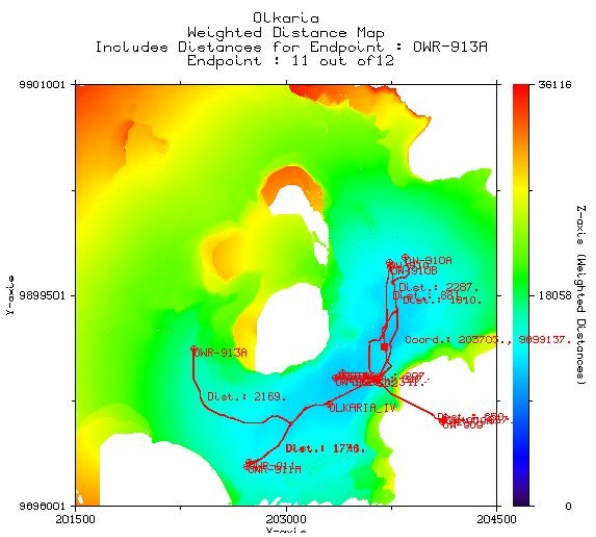

FIGURE 7: Distance map with new SD2 coordinates and distances to all routes

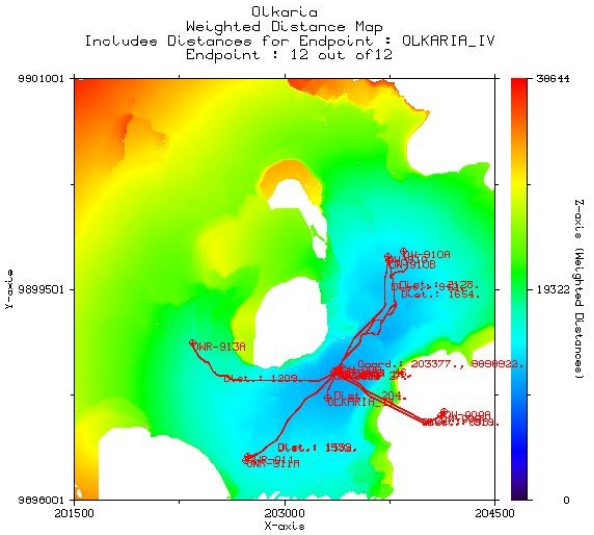

FIGURE 8: Olkaria IV distance map with modified route to OW913A, new SD2 coordinates and distances to all routes

on the number of separators in the field, the same procedure is repeated for all separators. An optimized location to place each separator is obtained and the route to each production, hot reinjection well and to the power plant is defined (Figure 7).

The digital maps generated as output are very interactive and allow one to make a decision whether there is still room for further optimization or not. As Figure 7 shows, the route to OW-913A can be further improved as indicated by the available blue coloured region in the weighted distance map. The route could still be optimized by allowing a little more slope difference and the results change as shown in Figure 8.

The final optimized routes and the location of power plant is achieved and results recorded in an output file. Table 7 summarizes the results. From the results it is clear that using this approach to locate the

TABLE 7: Results for pipeline route selection and separator location optimization

Wells/power plant	**Distance from initial location separator - SD2 (m)**	**Distance from optimized location separator - SD2 (m)**
908	297.40	45.76
908A	316.69	13.52
908B	341.11	26.82
909	649.90	897.92
909A	656.90	919.37
910	881.15	942.43
910A	2286.64	2127.65
910B	1810.46	1654.46
911	1743.72	1499.28
911A	1776.40	1531.96
913A	2168.85	1924.40
OLKARIA_IV	400.56	203.53
Total length	**13329.78**	**11787.1**
New optimized separator SD2 location coordinates		
Easting (X)	**Northing (Y)**	**Elevation (m a.s.l.)**
203375.00	9898916.00	2024.57

power plant leads to a reduction of pipeline length to 11,787.1 m compared to the initial length of 13,329.8 m. This result, while being correct, may not be entirely true as other parameters which were not considered in this optimization may have led to the current route being an option. However, given all constraints, this optimization approach could give accurate results.

4.3 Power plant placement and optimization

The inputs in this step take into account only the optimized coordinates of all separators as end points. The initial plant location then becomes the sample point. The necessary slope, height and weight constraints are then defined in the VTDISTRA. The input to the program is configured to accept plant given name as sample point without starting with initials, S_Name of plant as shown in Appendix III. The output is a weighted distance map (Figure 9) and weighted distance maps from each end point to

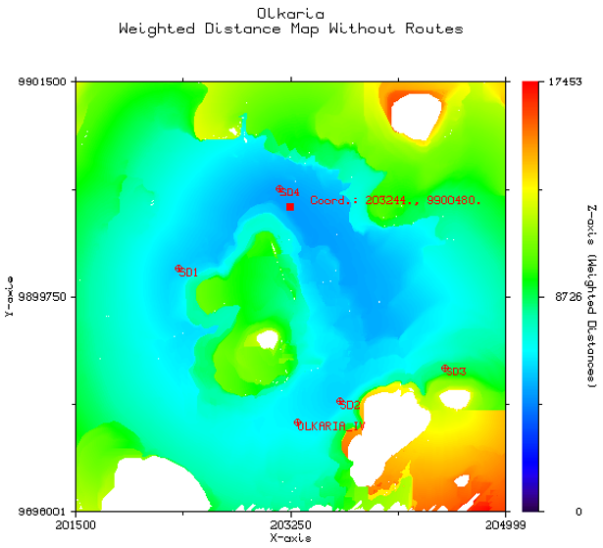

FIGURE 9: Olkaria 4 weighted distance map with optimized separators and current plant locations

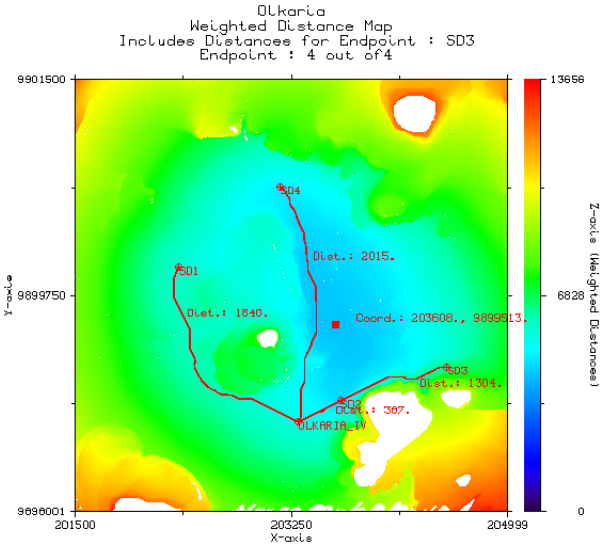

FIGURE 10: Olkaria 4 weighted distance map with routes to all separators and new coordinates for plant location

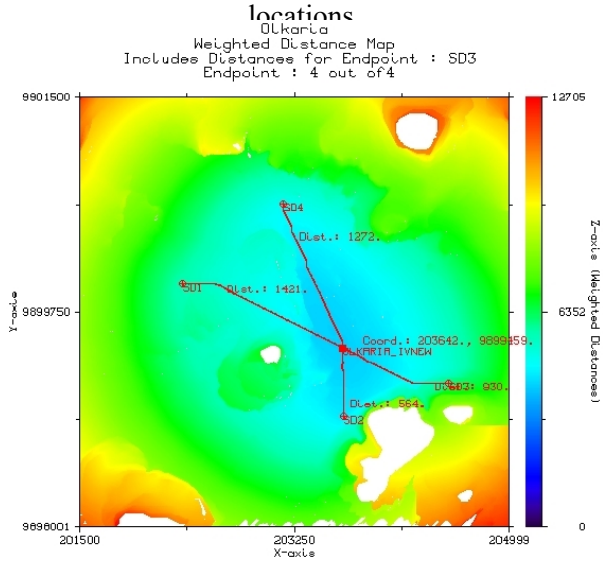

FIGURE 11: Olkaria 4 weighted distance map with routes to all separators and new coordinates for plant location

the sample point complete with routes and their distances. New optimized coordinates for the plant and distances to separators are displayed in the weighted distance map shown in Figure 10. Now using the new plant coordinates as the sample point and separator station coordinates as endpoints, VTDISTRA is run again to obtain the routes and distances to each of the endpoints. The output is captured in form of distance maps, weighted distance maps and an output file which captures the power plant optimized location coordinates and those of all routes sampled with one metre intervals. The new distances from each separator to the optimized power plant location and the coordinates for the optimized location are presented in Table 8. Figure 11 illustrates the graphical outcome of the plant location optimization.

TABLE 8: Results for power plant location optimization

Separators	**Run 1 (m)**	**Run 2 (m)**	**Run 3 (m)**	**Run 4 (m)**	**Run 5 (m)**
SD1	2681.67	2681.67	1840.00	1704.00	1420.92
SD2	386.74	386.74	386.74	386.74	563.55
SD3	No route	1303.00	1304.00	1296.00	929.51
SD4	4463.00	2014.95	2015.00	1923.00	1271.67
TOTAL		6386.36	5545.74	5310.00	**4185.65**
New optimized power plant coordinates					
Easting (X)		**Northing (Y)**		**Height (m a.s.l.)**	
203642.00		9899459.00		2008.72	

4.4 Separator and pipeline dimensional design and cost estimation

4.4.1 Separator dimensions

Separator dimensions are designed using the guidelines by Purnanto et al. (2012). The recommended velocity is selected as 40 m/s and results recorded are listed in Table 9.

Using the results from Spiral-inlet design formulas in Table 9, the separator thickness was evaluated. An attempt was made to calculate the separator thickness as if it was one unit and also a design for three separators was considered individually. Each possible layout of well combination serving each separator was followed and the cost of each separator was estimated. The results are presented in Table 10.

The full design results are found in Appendix V (a-d) together with separator design worksheets which show all parameters calculated including diameters and thicknesses.

TABLE 9: Results for separator design

Para-meter	**Bangma design**	**Lazalde-Crabtree design**	**Spiral-inlet design**
D	2.90	3.19	**2.8**
D_e	0.77	0.97	**1.00**
D_b	0.97	0.97	**0.70**
α	3.14	0.14	**0.3**
β	2.90	3.38	**3.10**
Z	2.90	5.31	**5.60**
L_T	6.76	6.25	**2.00**
L_B	4.35	4.80	**4.70**

TABLE 10: Results for separator thickness and cost estimation

Separator unit	**No. of wells**	**Steam mass flow rate (kg/s)**	**Thickness T (mm)**	**Weight (kg)**	**Cost (USD)**
SD2 (1 unit)	8	134.70	23	3566	12056
SD2A	4	40.83	7	548	1609
SD2B	2	57.72	16	2063	6209
SD2C	2	36.19	13	1548	4196

4.4.2 Results of pipeline design, optimization and cost

Pipeline dimensions are calculated separately for single-phase and two-phase flow pipes. Summary design results are presented in Table 11 while the full design results are presented in Appendix VI including a pipeline design worksheet.

TABLE 11: Calculated results of pipelines design and cost estimation

Pipeline	Total length (m)	Diameter D (mm)	Thickness (mm)	Weight (kg)	Cost (USD)
908-SD2A	45.76	200	15.09	3,474	6,531
908A-SD2B	14.00	250	18.26	1,551	2,963
908B-SD2C	26.82	300	31.44	6,082	11,920
909 & 909A-SD2	1654.00	450	29.37	512,752	1,389,558
910-SD2	898.00	250	18.26	103,038	196,802
910A-SD2	919.00	350	23.83	179,278	406,961
910B-SD2	942.00	450	29.37	292,079	791,534
SD2-911&	45.76	100	11.53	1,277	2,400
SD2-911A	46.76	400	30.96	133,323	34,017
SD2-913	47.76	300	21.44	7,638	15,032
SD1-OLK4	1420.90	350	6.35	70,662	160,403
SD2-OLK4	563.55	350	6.35	28,046	63,665
SD3-OLK4	929.51	350	6.35	46,246	10,4979
SD4-OLK4	1271.67	350	6.35	63,253	143,584
					(3,330,349)

5. CONCLUSIONS

A tool for optimizing route selection, separator and power plant placement has been developed. The tool was tested using data from Olkaria geothermal field and the best location of the separator and power plant were obtained together with the optimum pipeline route and total length of each route.

The study proposes a methodology where first the separator location is obtained using coordinates of all production and hot reinjection wells and an initial proposed power plant location. Using VTDT, a new optimized separator location and distance from each well to the plant is obtained. This process is repeated for all separators. The second process step involves plant location where only the optimized separator locations and any constrained areas are used as input in the VTDT program. The result is an optimized location of the plant coordinates and distances from the plant to each separator.

The use of WVTDT for route selection, separator and power plant location gives very good results that can be used to optimize steam systems in geothermal projects. The model developed can be modified to include further constraints to achieve a more acceptable or compromised route.

Using data for Olkaria IV geothermal field, the overall pipeline length reduced by 1542 m. This goes a long way in reducing cost of the pipeline. Accurate results can be achieved in any field by first carrying out a study including all the sensitive areas like protected wildlife breeding grounds and migratory routes, existing buildings and excessively harsh terrains which can then be excluded by introducing their coordinates as constraints.

This model and methodology can be useful in designing preliminary pipeline routes and locations for separators and power plants before detailed survey of the area and consideration of constraints is done. This can help in project planning and cost estimation.

While pipeline diameter and thickness were optimized in this study, it is important in a real case to always go an extra mile and calculate other pipeline design parameters like bending moments, length between pipe supports pipeline anchors and expansion loops which were not considered in this study.

ACKNOWLEDGEMENTS

Firstly, I would like to express my sincere gratitude to my project supervisor Professor Magnús Thór Jónsson for the continuous support, patience, and immense knowledge. Your availability and guidance helped me all the time. To my project mate Dan, thank you so much for your assistance.

I thank UNU-GTP and in particular the director, Lúdvík for giving me a chance to pursue this program in Iceland. To all the staff of UNU-GTP and ÍSOR you made me feel at home away from home. I thank my company KenGen, through the Geothermal Development Director, Eng. Abel Rotich for nominating and according me time of duty to study this course.

I would like to thank my colleagues of UNU-GTP 2016 for their wonderful collaboration and special moments shared. You were all always willing to help me. I trust that the contacts and network we have made will last through our future engagements. To the football team thank you so much for your time. To my housemates James and Gideon, the wonderful evenings we chatted, the 'Fiskur' and 'Jakuzi' experience were all moments to reckon. And to our landlord, Jóhann and family, thank you for allowing us to use the facilities in your apartment that made our stay in Sogavegur memorable.

To my dear wife Nelly and my lovely daughter Angela, those evening calls always rejuvenated my spirits and ensured I had a peaceful sleep every day! Thank you for your understanding and encouragement.

Last but not least I thank God for my life and good health and for blessing me with a beautiful family.

REFERENCES

ASME, 2007: *ASME B31.1-2007. Power piping.* The American Society of Mechanical Engineers, New York, NY, United States, 336 pp.

Bangma, P., 1961: The development and performance of a steam – water separator for use on geothermal bores. *Proceedings of the UN Conference on New Sources of Energy, Vol. 2, Geothermal Energy Agenda, item II.A.2*, 60-77.

de Smith, M.J., 2004: Distance transforms as a new tool in spatial analysis, urban planning, and GIS. *Environment and Planning, B: Planning and design, 31,* 85-104.

DiPippo, R., 2007: *Geothermal power plants. Principles, applications, case studies and environmental impact* (2nd ed.). Butterworth Heineman, Elsevier, 493 pp.

Gerunda, A., 1981: How to size liquid-vapour separators. *Chemical Engineering, 88*, 81-84.

GoK, 2014: *10-year power sector expansion plan 2014-2024.* Government of Kenya, report, 68 pp.

Henriquez M., J.L. and Aguirre A., L., 2011: Piping design, the fundamentals. *Paper presented at "Short Course on Geothermal Drilling, Resource Development and Power Plants", organized by UNU-GTP and LaGeo, in Santa Tecla, El Salvador,* 15 pp.

Hewitt, G.F., 1982: Pressure drop. In: Hetsroni, G. (ed.), *Handbook of multiphase systems*. Hemisphere, McGraw Hill, NY, United States, 2.44-2.75.

Kalinci, Y., Hepbasli, A., and Tavman, I., 2008: Determination of optimum pipe diameter along with energetic and exergetic evaluation of geothermal district heating systems: Modeling and application. *Energy and Buildings, 40,* 742–755.

Kristinsson, H., 2005: *Pipe route design using variable topography distance transforms.* University of

Iceland, Reykjavík, Iceland, 28 pp.

Jónsson, M.Th., 2016a: *Mechanical design of geothermal power plants and district heating systems.* UNU-GTP, Iceland, unpublished lecture notes, 79 pp.

Jónsson, M.Th., 2016b: *Design and optimization – distance transforms.* UNU-GTP, Iceland, unpublished lecture notes.

Lazalde-Crabtree, H., 1984: Design approach of steam-water separators and steam dryers for geothermal applications. *Geothermal Resource Council Bulletin, September 1984*, 11-20.

Lee, K.C., 1982: Performance tests of the condensate drain pots at Wairakei. *Proceedings of the Pacific Geothermal Conference, Wairakei, New Zealand*, 123–129.

Lee, K.C., 1995: Performance of a model in-line vortex separator: *Proceedings of the World Geothermal Congress 1995, Florence, Italy,* 2075-2079.

Mannvit, 2012: *Proposed field development plan for Greater Olkaria geothermal field*. Mannvit Consortium – consultancy services for geothermal resource optimisation study of Greater Olkaria geothermal fields, report 8, Kenya Electricity Generating Company Ltd. – KenGen, internal report, 59 pp.

Mwawongo, G.M, 2013: Geothermal mapping using temperature measurements. *Presented at "Short Course VIII on Exploration for Geothermal Resources", organized by UNU-GTP, GDC and KenGen, at Lake Bogoria and Lake Naivasha, Kenya,* 13 pp.

Nag, P.K., 2008: *Power plant engineering* (3rd ed.). Tata, McGraw Hill, New Delhi, India, 478-539.

Onyango, S.O., 2015: *Design of steam gathering system for Menengai geothermal field, Kenya.* University of Iceland, MSc thesis, UNU-GTP report 1-2015, 71 pp.

Ouma, P.A, 1992: *Steam gathering system for NE-Olkaria geothermal field, Kenya – preliminary design.* United Nations University Geothermal Training Programme, Reykjavík, Iceland, report 9, 46 pp.

Pálsson, H., Bergthórsson E.S., and Pálsson O.P., 2006: Estimation and validation of models of two phase flow from geothermal wells. *Paper presented at 10th International Symposium on District Heating and Cooling, Hanover, Germany,* 11 pp.

Purnanto, M.H., Zarrouk, S.J., and Cater, J.E., 2012: CFD modelling of two-phase flows inside geothermal steam-water separators. *Proceedings of the 34th New Zealand Geothermal Workshop, University of Auckland, Auckland, New Zealand,* 9 pp.

Riaroh, D. and Okoth, W., 1996: The geothermal fields of the Kenya rift. *Tectonophysics, 236,* 117-130.

Tioga Pipe, 2014: *Pipe thicknesses.* Tioga Pipe – pipe supply company, PH, USA, website: *www.tiogapipe.com.*

Valdimarsson, P., 2010: Production of electricity from a geothermal source. In: *Geothermal Energy*. Macedonian Geothermal Association (MAGA), Skopje, 150-176 pp.

Watson, A., Brodie, A.J., and Lory, P.J., 1996: The process design of steam fields pipeline systems for transient operation from liquid dominated reservoirs. *Proceedings of the 18th New Zealand Geothermal Workshop, Auckland, New Zealand,* 53-58.

Zhao, H., Lee, K., and Freeston, D., 2000: Geothermal two-phase flow in horizontal pipes. *Proceedings of the World Geothermal Congress, 2000, Kyushu-Tohoku, Japan,* 3349-3353.

APPENDIX I: Pipe thicknesses and costs (Tioga, 2014)

Tioga™

Philadelphia Regional Center
2450 Wheatsheaf Lane
Philadelphia, PA 19137
O 215-831-0700
F 215-533-1645
E sales@tiogapipe.com

Houston Regional Center
616 FM 1960 W, Suite 700
Houston, TX 77090
O 713-433-2111
F 281-397-0132
E sales@tiogapipe.com

Chattanooga Regional Center
1301 Riverfront Parkway, Suite 108
Chattanooga, TN 37402
O 423-899-3398
F 423-899-9695
E sales@tiogapipe.com

PIPE DIMENSIONS AND WEIGHTS

Available in commercial and nuclear

U.S./METRIC

NOMINAL PIPE SIZE	OD	SCHEDULE DESIGNATIONS			WALL THICKNESS		WEIGHT		ID	
INCH / MM	INCH / MM	ASME			INCH	MM	LBS/FOOT	KG/METER	INCH	MM
1/8 / 6	0.405 / 10.3	10		10S	0.049	1.24	0.19	0.28	0.307	7.82
		STD	40	40S	0.068	1.73	0.24	0.37	0.269	6.84
		XS	80	80S	0.095	2.41	0.31	0.47	0.215	5.84
1/4 / 8	0.540 / 13.7	10		10S	0.065	1.65	0.33	0.49	0.410	10.40
		STD	40	40S	0.088	2.24	0.43	0.63	0.364	9.22
		XS	80	80S	0.119	3.02	0.54	0.80	0.302	7.66
3/8 / 10	0.675 / 17.1	10		10S	0.065	1.65	0.42	0.63	0.545	13.80
		STD	40	40S	0.091	2.31	0.57	0.84	0.493	12.48
		XS	80	80S	0.126	3.20	0.74	1.10	0.423	10.70
1/2 / 15	0.840 / 21.3	5		5S	0.065	1.65	0.54	0.80	0.710	18.00
		10		10S	0.083	2.11	0.67	1.00	0.674	17.08
		STD	40	40S	0.109	2.77	0.85	1.27	0.622	15.76
		XS	80	80S	0.147	3.73	1.09	1.62	0.546	13.84
		160			0.188	4.78	1.31	1.95	0.464	11.74
		XX			0.294	7.47	1.72	2.55	0.252	6.36
3/4 / 20	1.050 / 26.7	5		5S	0.065	1.65	0.69	1.03	0.920	23.40
		10		10S	0.083	2.11	0.86	1.28	0.884	22.48
		STD	40	40S	0.113	2.87	1.13	1.69	0.824	20.96
		XS	80	80S	0.154	3.91	1.48	2.20	0.742	18.88
		160			0.219	5.56	1.95	2.90	0.612	15.58
		XX			0.308	7.82	2.44	3.64	0.434	11.06
1 / 25	1.315 / 33.4	5		5S	0.065	1.65	0.87	1.29	1.185	30.10
		10		10S	0.109	2.77	1.41	2.09	1.097	27.86
		STD	40	40S	0.133	3.38	1.68	2.50	1.049	26.64
		XS	80	80S	0.179	4.55	2.17	3.24	0.957	24.30
		160			0.250	6.35	2.85	4.24	0.815	20.70
		XX			0.358	9.09	3.66	5.45	0.599	15.22
1-1/4 / 32	1.660 / 42.2	5		5S	0.065	1.65	1.11	1.65	1.530	38.90
		10		10S	0.109	2.77	1.81	2.69	1.442	36.66
		STD	40	40S	0.140	3.56	2.27	3.39	1.380	35.08
		XS	80	80S	0.191	4.85	3.00	4.47	1.278	32.50
		160			0.250	6.35	3.77	5.61	1.160	29.50
		XX			0.382	9.70	5.22	7.77	0.896	22.80
1-1/2 / 40	1.900 / 48.3	5		5S	0.065	1.65	1.28	1.90	1.770	45.00
		10		10S	0.109	2.77	2.09	3.11	1.682	42.76
		STD	40	40S	0.145	3.68	2.72	4.05	1.610	40.94
		XS	80	80S	0.200	5.08	3.63	5.41	1.500	38.14
		160			0.281	7.14	4.86	7.25	1.338	34.02
		XX			0.400	10.15	6.41	9.55	1.100	28.00
2 / 50	2.375 / 60.3	5		5S	0.065	1.65	1.61	2.39	2.245	57.00
		10		10S	0.109	2.77	2.64	3.93	2.157	54.76
		STD	40	40S	0.154	3.91	3.66	5.44	2.067	52.48
		XS	80	80S	0.218	5.54	5.03	7.48	1.939	49.22
		160			0.344	8.74	7.47	11.11	1.687	42.82
		XX			0.436	11.07	9.04	13.44	1.503	38.16
2-1/2 / 65	2.875 / 73.0	5		5S	0.083	2.11	2.48	3.69	2.709	68.78
		10		10S	0.120	3.05	3.53	5.26	2.635	66.90
		STD	40	40S	0.203	5.16	5.80	8.63	2.469	62.68
		XS	80	80S	0.276	7.01	7.67	11.41	2.323	58.98
		160			0.375	9.53	10.02	14.92	2.125	53.94
		XX			0.552	14.02	13.71	20.39	1.771	44.96
3 / 80	3.500 / 88.9	5		5S	0.083	2.11	3.03	4.52	3.334	84.68
		10		10S	0.120	3.05	4.34	6.46	3.260	82.80
		STD	40	40S	0.216	5.49	7.58	11.29	3.068	77.92
		XS	80	80S	0.300	7.62	10.26	15.27	2.900	73.66
		160			0.438	11.13	14.34	21.35	2.624	66.64
		XX			0.600	15.24	18.60	27.68	2.300	58.42
3-1/2 / 90	4.000 / 101.6	5		5S	0.083	2.11	3.48	5.18	3.834	97.38
		10		10S	0.120	3.05	4.98	7.41	3.760	95.50
		STD	40	40S	0.226	5.74	9.12	13.57	3.548	90.12
		XS	80	80S	0.318	8.08	12.52	18.64	3.364	85.44
		XX			0.636	16.15	22.87	34.03	2.728	69.30
4 / 100	4.500 / 114.3	5		5S	0.083	2.11	3.92	5.84	4.334	110.08
		10		10S	0.120	3.05	5.62	8.37	4.260	108.20
					0.156	3.96	7.24	10.78	4.188	106.38
					0.188	4.78	8.67	12.91	4.124	104.74
		STD	40	40S	0.237	6.02	10.80	16.08	4.026	102.26
		XS	80	80S	0.337	8.56	15.00	22.32	3.826	97.18
		120			0.438	11.13	19.02	28.32	3.624	92.04
		160			0.531	13.49	22.53	33.54	3.438	87.32
		XX			0.674	17.12	27.57	41.03	3.152	80.06
4-1/2 / 115	5.000 / 127.0	STD	40	40S	0.247	6.27	12.55	18.67	4.506	114.46
		XS	80	80S	0.355	9.02	17.63	26.24	4.290	108.96
		XX			0.710	18.03	32.56	48.45	3.580	90.94

NOMINAL PIPE SIZE	OD	SCHEDULE DESIGNATIONS			WALL THICKNESS		WEIGHT		ID	
INCH / MM	INCH / MM	ASME			INCH	MM	LBS/FOOT	KG/METER	INCH	MM
5 / 125	5.563 / 141.3	5		5S	0.109	2.77	6.36	9.46	5.345	135.76
		10		10S	0.134	3.40	7.78	11.56	5.295	134.50
		STD	40	40S	0.258	6.55	14.63	21.77	5.047	128.20
		XS	80	80S	0.375	9.53	20.80	30.97	4.813	122.24
		120			0.500	12.70	27.06	40.28	4.563	115.90
		160			0.625	15.88	32.99	49.12	4.313	109.54
		XX			0.750	19.05	38.59	57.43	4.063	103.20
6 / 150	6.625 / 168.3	5		5S	0.109	2.77	7.59	11.31	6.407	162.76
		10		10S	0.134	3.40	9.30	13.83	6.357	161.50
					0.188	4.78	12.94	19.28	6.249	158.74
		STD	40	40S	0.280	7.11	18.99	28.26	6.065	154.08
		XS	80	80S	0.432	10.97	28.60	42.56	5.761	146.36
		120			0.562	14.27	36.43	54.21	5.501	139.76
		160			0.719	18.26	45.39	67.57	5.187	131.78
		XX			0.864	21.95	53.21	79.22	4.897	124.40
7 / 175	7.625 / 193.7	STD	40	40S	0.301	7.65	23.57	35.10	7.023	178.40
		XS	80	80S	0.500	12.70	38.08	56.69	6.625	168.30
		XX			0.875	22.23	63.14	94.00	5.875	149.24
8 / 200	8.625 / 219.1			5S	0.109	2.77	9.92	14.78	8.407	213.56
		10		10S	0.148	3.76	13.41	19.97	8.329	211.58
		20			0.250	6.35	22.38	33.32	8.125	206.40
		30			0.277	7.04	24.72	36.82	8.071	205.02
		STD	40	40S	0.322	8.18	28.58	42.55	7.981	202.74
		60			0.406	10.31	35.67	53.09	7.813	198.48
		XS	80	80S	0.500	12.70	43.43	64.64	7.625	193.70
		100			0.594	15.09	51.00	75.92	7.437	188.92
		120			0.719	18.26	60.77	90.44	7.187	182.58
		140			0.812	20.62	67.82	100.93	7.001	177.86
		XX			0.875	22.23	72.49	107.93	6.875	174.64
		160			0.906	23.01	74.76	111.27	6.813	173.08
9 / 225	9.625 / 244.5	STD	40	40S	0.342	8.69	33.94	50.54	8.941	227.12
		XS	80	80S	0.500	12.70	48.77	72.60	8.625	219.10
		XX			0.875	22.23	81.85	121.85	7.875	200.04
10 / 250	10.750 / 273.0			5S	0.134	3.40	15.21	22.61	10.482	266.20
				10S	0.165	4.19	18.67	27.78	10.420	264.62
					0.188	4.78	21.23	31.62	10.374	263.44
		20			0.250	6.35	28.06	41.76	10.250	260.30
		30			0.307	7.80	34.27	51.01	10.136	257.40
		STD	40	40S	0.365	9.27	40.52	60.29	10.020	254.46
		XS	60	80S	0.500	12.70	54.79	81.53	9.750	247.60
		80			0.594	15.09	64.49	95.98	9.562	242.82
		100			0.719	18.26	77.10	114.71	9.312	236.48
		120			0.844	21.44	89.38	133.01	9.062	230.12
		140	XX		1.000	25.40	104.23	155.10	8.750	222.20
		160			1.125	28.58	115.75	172.27	8.500	215.84
11 / 275	11.750 / 298.5	STD	40	40S	0.375	9.53	45.60	67.91	11.000	279.44
		XS	80	80S	0.500	12.70	60.13	89.51	10.750	273.10
		XX			0.875	22.23	101.72	151.46	10.000	254.04
12 / 300	12.750 / 323.8			5S	0.156	3.96	21.00	31.24	12.438	315.88
				10S	0.180	4.57	24.19	35.98	12.390	314.66
					0.188	4.78	25.25	37.61	12.374	314.24
		20			0.250	6.35	33.41	49.71	12.250	311.10
		30			0.330	8.38	43.81	65.19	12.090	307.04
		STD		40S	0.375	9.53	49.61	73.86	12.000	304.74
		40			0.406	10.31	53.57	79.71	11.938	303.18
		XS		80S	0.500	12.70	65.48	97.44	11.750	298.40
		60			0.562	14.27	73.22	108.93	11.626	295.26
		80			0.688	17.48	88.71	132.05	11.374	288.84
		100			0.844	21.44	107.42	159.87	11.062	280.92
		120	XX		1.000	25.40	125.61	186.92	10.750	273.00
		140			1.125	28.58	139.81	208.08	10.500	266.64
		160			1.312	33.32	160.42	238.69	10.126	257.16
14 / 350	14.000 / 355.6			10S	0.188	4.78	27.76	41.36	13.624	346.04
		10			0.250	6.35	36.75	54.69	13.500	342.90
		20			0.312	7.92	45.65	67.91	13.376	339.76
		STD	30	40S	0.375	9.53	54.62	81.33	13.250	336.54
		40			0.438	11.13	63.50	94.55	13.124	333.34
		XS		80S	0.500	12.70	72.16	107.40	13.000	330.20
		60			0.594	15.09	85.13	126.72	12.812	325.42
		80			0.750	19.05	106.23	158.11	12.500	317.50
		100			0.938	23.83	130.98	194.98	12.124	307.94
		120			1.094	27.79	150.93	224.66	11.812	300.02
		140			1.250	31.75	170.37	253.58	11.500	292.10
		160			1.406	35.71	189.29	281.72	11.188	284.18

NOMINAL PIPE SIZE	OD	SCHEDULE DESIGNATIONS	WALL THICKNESS		WEIGHT		ID	
INCH MM	INCH MM	ASME	INCH	MM	LBS/ FOOT	KG/ METER	INCH	MM
16 400	16.000 406.4	10S 10 20 STD 30 40S XS 40 80S 60 80 100 120 140 160	0.188 0.250 0.312 0.375 0.500 0.656 0.844 1.031 1.219 1.438 1.594	4.78 6.35 7.92 9.53 12.70 16.66 21.44 26.19 30.96 36.53 40.49	31.78 42.09 52.32 62.64 82.85 107.60 136.74 164.98 192.61 223.85 245.48	47.34 62.65 77.83 93.27 123.31 160.13 203.54 245.57 286.66 333.21 365.38	15.624 15.500 15.376 15.250 15.000 14.688 14.312 13.938 13.562 13.124 12.812	396.84 393.70 390.56 387.34 381.00 373.08 363.52 354.02 344.48 333.34 325.42
18 450	18.000 457	10S 10 20 STD 40S 30 XS 80S 40 60 80 100 120 140 160	0.188 0.250 0.312 0.375 0.438 0.500 0.562 0.750 0.938 1.156 1.375 1.562 1.781	4.78 6.35 7.92 9.53 11.13 12.70 14.27 19.05 23.83 29.36 34.93 39.67 45.24	35.80 47.44 58.99 70.65 82.23 93.54 104.76 138.30 171.08 208.15 244.37 274.48 308.79	53.31 70.57 87.71 105.17 122.38 139.16 155.81 205.75 254.57 309.64 363.58 408.28 459.39	17.624 17.500 17.376 17.250 17.124 17.000 16.876 16.500 16.124 15.688 15.250 14.876 14.438	447.44 444.30 441.16 437.94 434.74 431.60 428.46 418.90 409.34 398.28 387.14 377.66 366.52
20 500	20.000 508	10S 10 STD 20 40S XS 30 80S 40 60 80 100 120 140 160	0.218 0.250 0.375 0.500 0.594 0.812 1.031 1.281 1.500 1.750 1.969	5.54 6.35 9.53 12.70 15.09 20.62 26.19 32.54 38.10 44.45 50.01	46.10 52.78 78.67 104.23 123.23 166.56 209.06 256.34 296.65 341.41 379.53	68.61 78.56 117.15 155.13 183.43 247.84 311.19 381.55 441.52 508.15 564.85	19.564 19.500 19.250 19.000 18.812 18.376 17.938 17.438 17.000 16.500 16.062	496.92 495.30 488.94 482.60 477.82 466.76 455.62 442.92 431.80 419.10 407.98
22 550	22.000 559	10S 10 STD 20 40S XS 30 80S 60 80 100 120 140 160	0.218 0.250 0.375 0.500 0.875 1.125 1.375 1.625 1.875 2.125	5.54 6.35 9.53 12.70 22.23 28.58 34.93 41.28 47.63 53.98	50.76 58.13 86.69 114.92 197.60 251.05 303.16 353.94 403.38 451.49	75.55 86.55 129.14 171.10 294.27 373.85 451.45 527.05 600.67 672.30	21.564 21.500 21.250 21.000 20.250 19.750 19.250 18.750 18.250 17.750	547.92 546.30 539.94 533.60 514.54 501.84 489.14 476.44 463.74 451.04

NOMINAL PIPE SIZE	OD	SCHEDULE DESIGNATIONS	WALL THICKNESS		WEIGHT		ID	
INCH MM	INCH MM	ASME	INCH	MM	LBS/ FOOT	KG/ METER	INCH	MM
24 600	24.000 610	10 10S STD 20 40S XS 80S 30 40 60 80 100 120 140 160	0.250 0.375 0.500 0.562 0.688 0.969 1.219 1.531 1.812 2.062 2.344	6.35 9.53 12.70 14.27 17.48 24.61 30.96 38.89 46.02 52.37 59.54	63.47 94.71 125.61 140.81 171.45 238.57 296.86 367.74 429.79 483.57 542.64	94.53 141.12 187.07 209.65 255.43 355.28 442.11 547.74 640.07 720.19 808.27	23.500 23.250 23.000 22.876 22.624 22.062 21.562 20.938 20.376 19.876 19.312	597.30 590.94 584.60 581.46 575.04 560.78 548.08 532.22 517.96 505.26 490.92
26 650	26.000 660	10 STD 40S XS 80S	0.312 0.375 0.500	7.92 9.53 12.70	85.68 102.72 136.30	127.36 152.88 202.74	25.376 25.250 25.000	644.16 640.94 634.60
28 700	28.000 711	10 STD 40S XS 20 80S 30	0.312 0.375 0.500 0.625	7.92 9.53 12.70 15.88	92.35 110.74 146.99 182.90	137.32 164.86 218.71 272.23	27.376 27.250 27.000 26.750	695.16 691.94 685.60 679.24
30 750	30.000 762	10 STD 40S XS 20 80S 30	0.312 0.375 0.500 0.625	7.92 9.53 12.70 15.88	99.02 118.76 157.68 196.26	147.29 176.85 234.68 292.20	29.376 29.250 29.000 28.750	746.16 742.94 736.60 730.24
32 800	32.000 813	10 STD XS 20 30 40	0.312 0.375 0.500 0.625 0.688	7.92 9.53 12.70 15.88 17.48	105.69 126.78 168.37 209.62 230.29	157.25 188.83 250.65 312.17 342.94	31.376 31.250 31.000 30.750 30.624	797.16 793.94 787.60 781.24 778.04
34 850	34.000 864	10 STD XS 20 30 40	0.312 0.375 0.500 0.625 0.688	7.92 9.53 12.70 15.88 17.48	112.36 134.79 179.06 222.99 245.00	167.21 200.82 266.63 332.14 364.92	33.376 33.250 33.000 32.750 32.624	848.16 844.94 838.60 832.24 829.04
36 900	36.000 914	10 STD XS	0.312 0.375 0.500	7.92 9.53 12.70	119.03 142.81 189.75	176.97 212.57 282.29	35.376 35.250 35.000	898.16 894.94 888.60
42 1050	42.000 1067	STD XS	0.375 0.500 0.625 0.750	9.53 12.70 15.88 19.05	166.86 221.82 276.44 330.72	248.53 330.21 411.64 492.33	41.250 41.000 40.750 40.500	1047.94 1041.60 1035.24 1028.90
48 1200	48.000 1219	STD XS	0.375 0.500	9.53 12.70	190.92 253.89	284.25 377.81	47.250 47.000	1199.94 1193.60

PIPING • TUBING • FITTINGS FLANGES • RELATED PRODUCTS

Type	Seamless & Welded
Commodity	Chrome • Stainless • Carbon • Low Temperature
Specifications	A/SA335 • A/SA312 • A/SA213 • A/SA106 • A/SA53/API5L • A/SA333
Sizes (O.D.)	1/8" (3.175mm) - 60" (1524mm) (Larger ODs Available)
Grades	Chrome: P1 • P5 • P9 • P11 • P22 • P91 Stainless: 304 • 304H • 304L • 316 • 316H • 316L • 316LN • 321 • 321H • 347 • 347H • 310 • 310s • 309 • Alloy 20 Low Temp: Grade 1/6 • Grade 3 Carbon: Grade B • Grade C • Galvanized

MILITARY SPEC PIPE & TUBING

Program	MIL-I-45208A Quality Program • Approved Level 1 Supplier
Contact Tioga for	U.S. Navy Specifications • Navy Nuclear • MIC Level 1 • Ultrasonic Testing
Fittings & Flanges	All Fittings & Flanges to Match the Pipe

NUCLEAR MATERIALS

Program	ASME Section III - ASME QSC 467
Specifications	10CFR50 Appendix B • N45.2 • NQA-1 • U.S. Navy Nuclear Specifications
Products	Pipe • Tubing • Fittings • Flanges • Structurals • Fasteners • Forgings • Castings • Weld Rod • Plate
Grades	Carbon • Stainless • Chrome Moly • Nickel Alloys • Duplex • 6 Moly Alloys • Low Temperature • Special Melts • Copper & Titanium

SPECIALTY ALLOYS

Type	Seamless & Welded
Commodity	Nickel • Duplex & Titanium
Specifications & Grades	Alloy 800 • Alloy 825 • Alloy 600 • Alloy 625 • Alloy 400 • 6% Moly Grades • Duplex A790 UNS 31803 • 316LN
Sizes (O.D.)	1/8" (3.175mm) - 8" (203.2mm)
Wall Dimensions	0.035" (.889mm) - 0.875" (22.23mm)

TIOGA SPECIALTIES

- Project Management
- 24/7 Emergency Service
- Just-In-Time Programs
- Inventory in Stock
- All Schedule Walls
- Special Heavy Walls to 4" (101.6mm)
- Header Pipe to 4" Wall (101.6mm)
- Special Intermediate Walls
- Average & Minimum Walls
- Saw Cut up to 40" (1016mm)
- Cutting: Square & Miter
- Custom Lengths and OD's
- End Preps-Various
- Hard to Find Metals & Sizes
- Se Habla Español
- Exceptional Mill/Sourcing Relations
- Dedicated Project Solution Teams
- Vendor Managed Inventory Programs
- Mobile On-Site Inventory Programs
- Quick Response Programs
- Low Total Cost Solutions
- International Export & Packaging
- EN PED 97/23/EC
- ISO 9001-2008
- MIC Level 1 Supplier
- In-House Testing
- Destructive Examination
- Non-Destructive Examination
- In-House Hydrostatic Testing
- Full EDI Capabilities
- Customized e-business Solutions
- Emergency Forged and Buttweld Fittings

Note: Actual dimensions can vary from the figures based on specifications/manufacturing tolerances. The Data for weight is based on the following calculation for wrought steel pipe:
LB/Foot = (Outside diameter [in.] – Wall Thickness [in.]) x (Wall Thickness [in.]) x (10.69)
KG/Meter = (Outside diameter [mm] – Wall Thickness [mm]) x (Wall Thickness [mm]) x (0.0246615)

When it has to be right.™

Call the center of your choice for our 24-hour emergency service

tiogapipe.com

Tioga™

APPENDIX II: Summary data for wells serving separator SD2

Well ID / Type	Northing (m)	Easting (m)	Elevation (m)	Rated output MW
Production				
OW-903A	202839.139	9899769.92	2042.982	4.5
OW-903B	202923.868	9899823.513	2046.225	4.0
OW-904	202472.42	9899973.375	2004.042	5.2
OW-904A	202481.75	9900131.597	1988.862	5.5
OW-904B	202506.899	9899988.952	2003.995	5.0
OW-907A	203113.003	9900635.792	1973.286	8.0
OW-908	203404.234	9898951	2013.65	4.0
OW-908A	203378.169	9898929.201	2013.475	6.0
OW-908B	203348.999	9898911.173	2013.181	8.8
OW-909	204115.88	9898603.874	2088.06	12.5
OW-909A	204138.056	9898631.681	2088.194	10.2
OW-910	203733.158	9899737.594	1994.956	4.6
OW-910A	203847.998	9799774.438	1986.917	13.0
OW-910B	203745.908	9899703.351	1994.977	14.9
OW-912	204602.369	9898181.674	2073.471	5.1
OW-912A	204634.343	9898198.266	2073.497	7.9
OW-915	204327.366	9900010.083	1980.541	7.5
OW-915A	204308.619	9899978.968	1980.584	13.0
OW-915B	204342.441	9900093.36	1980.53	10.5
OW-916	204858.848	9899094.309	2035.621	16.0
OW-916A	204879.446	9899063.912	2035.637	7.7
Hot reinjection	**Northing (m)**	**Easting (m)**	**Elevation (m)**	**Injection capacity (t/h)**
OW-901	201857.61	9900842.957	1891.762	
OW-902	201681.992	9899012.784	1951.568	300
OW-906	**201803**	**9899830**	**1974.8**	**645**
OW-906A	201724.686	9899916.941	1964.14	
OW-911	202736.133	9898315.193	1979.506	308
OW-911A	202725.67	9898287.453	1979.519	
OW-913A	202341.87	9899117.509	1980.837	
Cold reinjection	**Northing (m)**	**Easting (m)**	**Elevation (m)**	**Injection capacity (t/h)**
OW-902A	201788.014	9899062.327	1953.873	900
OW-902B	201801.32	9899032.181	1953.891	420

Note: Well OW906 has been earmarked for conversion from reinjection to production, hence it will not be considered in this study during optimization.

APPENDIX III: Sample input file for the VTDISTRA software

The file left behind has a .inp extension, and we cannot open it. The appendix should preferably not be longer than 1 page.

```
Title: Olkaria;

Output Device, Monitor/Gif/WMF/PDF (0/1/2/3): 1;
Color for marks, lines (0 Black/1 Red) (0/1): 1;
Draw Digital Elevation Map                      (0/1): 1;
Draw Distance Map (DM) Without Routes           (0/1): 1;
Draw DM, each with Route from nearest Endpoint (0/1): 1;
Draw DM with Routes from nearest Endpoint       (0/1): 1;
Draw DM with Routes to CP from Each Endpoint    (0/1): 1;
Draw Weighted Distance Map Without Routes       (0/1): 1;
Draw Weighted DM with Routes from Each Endpoint(0/1): 1;
Print Result File (0/1): 1;

Max height differences: 0.15;
Max allowable slope upward (ratio): 0.04;

Coordinates for Area Under Consideration A_Name:xmin;ymin;xmax;ymax
A_Olkaria IV: 201500.0; 9799000.0; 204500.0;   9902500.0;

Digital Elevation Matrix: Olkaria.dem;

Result file: Okaria.out;

Coordinates for Constraint Area C_Name:xmin;ymin;xmax;ymax
XC_A1: 201500.0; 9898500.0; 202000.0; 9899000.0;

Coordinates for Endpoints E_Name:X;Y;Z;w;maxh;maxs;
E_OW-908:  203404.234; 9898951.000; 2013.650;
E_OW-908A: 203378.169; 9898929.201; 2013.475;
E_OW-908B: 203348.999; 9898911.173; 2013.181;
E_OW-909:  204115.880; 9898603.874; 2088.060;
E_OW-909A: 204138.056; 9898631.681; 2088.194;
E_OW-910:  203733.158; 9899737.594; 1994.956; 1.0;  0.2; 0.1;
E_OW-910A: 203847.998; 9899774.438; 1986.917;
E_OW-910B: 203745.908; 9899703.351; 1994.977;
E_OWR-911: 202736.133; 9898315.193; 1979.506;
E_OWR-911A: 202725.67; 9898287.453; 1979.519;
E_OWR-913A: 202341.87; 9899117.509; 1980.837; 1.0; 0.2; 0.1;
E_OLKARIA_IV: 203306.0; 9898726.0; 1500.0;

Coordinates for Sample Points S_Name:X;Y;Z; (Separators, Powerplant)
S_SD2NEW: 203375.00; 9898916.00; 20224.57;
```

APPENDIX IV: Sample output file for the VTDISTRA software

The file left behind has a .out extension. When opened in Notepad and copied to Word, the information spreads over 83 pgs. Perhaps it is enough to show a sample? The appendix should preferably not be longer than 1 page, so this needs to be edited or opened differently.

```
Title: Olkaria

Matrix size (nx ny):         3001         3001
Area dim xmi xma dx:    201500.00    204500.00         1.00
Area dim ymi yma dy:   9898001.00   9901001.00         1.00
Height  (Hmin Hmax):      1760.00      2100.00
Crit. Height Slope :         0.150        0.040
Coord. heighest poin    203957.00   9898854.00      2100.00
Coord. s. weigh dist    203377.00   9898922.00      2024.74

 Route coordinates for shortest dist. Form To:
 Number of places To   :            1
 Number of places From :           12
 Route number     :           1           1
   Route from:  OW-908
   Route to   :  SD2NEW
   Distance   :         45.76
 No.   points:           28
    2   203375.00  9898916.00     2024.57
    3   203376.00  9898917.00     2024.61
    4   203377.00  9898918.00     2024.64
    5   203378.00  9898919.00     2024.68
    6   203379.00  9898920.00     2024.71
    7   203380.00  9898921.00     2024.74
    8   203381.00  9898922.00     2024.78
    9   203382.00  9898923.00     2024.81
   10   203383.00  9898924.00     2024.84
   11   203385.00  9898926.00     2024.91
   12   203386.00  9898927.00     2024.94
   13   203387.00  9898928.00     2024.98
   14   203388.00  9898929.00     2025.01
   15   203389.00  9898930.00     2025.04
   16   203390.00  9898931.00     2025.08
   17   203391.00  9898932.00     2025.11
   18   203392.00  9898933.00     2025.14
   19   203393.00  9898934.00     2025.18
   20   203394.00  9898935.00     2025.08
   21   203395.00  9898936.00     2025.11
   22   203397.00  9898938.00     2025.18
   23   203398.00  9898939.00     2025.21
   24   203399.00  9898941.00     2025.27
   25   203400.00  9898943.00     2025.33
   26   203401.00  9898945.00     2025.39
   27   203402.00  9898947.00     2025.45
   28   203403.00  9898949.00     2025.50
   29   203404.00  9898951.00     2025.56
 ***************************************************
```

APPENDIX V: Design results for the separator dimensions

Appendix Va - Separator Design Work Sheet				
Case of combined separator SD2				
Separation Pressure	1,2	mPa		
Steam Density@12bar	6,13	kg/m3		
Water Density@12bar	878,4	kg/m3		
Design Pressure CL150	2,0	mPa	Design pressure for Class 150 = 20 bar	
Mass flow rate steam, m	134,7	kg/s		
Volumetric flow rate, Qvs	21,97	m3/s		
Steam velocity (outlet)	40	m/s		
Flow Area, A	0,549	m3		
Diameter, Dt	0,836	m	Selected diameter DN850	
	Bangma	**Lazalde -Crabtree**	**Spiral Inlet**	
D	2,51	2,76	**2,5**	m
D_e	0,67	0,84	**0,8**	m
D_b	0,84	0,84	**0,6**	m
α	2,72	0,13	**0,2**	m
β	2,51	2,93	**2,7**	m
Z	2,51	4,60	**4,9**	m
L_T	5,85	5,41	**2,0**	m
L_B	3,76	4,16	**4,1**	m
Separator Wall Thickness				
Allowable Stress, S	122	mPa	17.7 ksi	(1 ksi = 6.895 mPa)
Welding Factor, E	1			
Temperature cofficient, y	0,4			
Corrosion Allowance, A	0,003			m
	Bangma	**Lazalde -Crabtree**	**Spiral Inlet**	
Minimum thickness, tm	0,023	0,025	0,023	m
Nominal Thickness 12.7mm MAX AS PER STEEL SCHEDULES				
Overal height, H	9,62	9,58	6,14	m
Ellipse short radius, b	0,63	0,69	-3,04	m
Ellipse long radius, a	1,25	1,38	1,23	m
Ellipse Surface Area	2,47	2,99	-11,80	m2
Cylinder Surface Area	75,81	83,03	47,58	m2
Total Surface Area	78,28	86,02	35,78	m2
Volume of Steel, V	0,99	1,09	0,45	m3
Density of steel	7850			kg/m3
Weight of steel (rhoX volume)	7804,33	8575,72	3566,72	kg
Cost/kg	3,38			USD/kg
Total Cost	26378,62	28985,94	12055,50	USD

Appendix Vb				
Separator Design Work Sheet - Case of SD2c unit				
Separation Pressure	1,2	mPa		
Steam Density@12bar	6,13	kg/m3		
Water Density@12bar	878,4	kg/m3		
Design Pressure CL150	2,0	mPa	Design pressure for Class 150 = 20 bar	
Mass flow rate steam, m	5,9	kg/s		
Volumetric flow rate, Qvs	0,96	m3/s		
Steam velocity (outlet)	40	m/s		
Flow Area, A	0,024	m3		
Diameter, Dt	0,175	m	Selected diameter DN200	
	Bangma	**Lazalde -Crabtree**	**Spiral Inlet**	
D	0,53	0,58	**0,5**	m
D_e	0,14	0,18	**0,2**	m
D_b	0,18	0,18	**0,1**	m
α	0,57	0,03	**0,0**	m
β	0,53	0,61	**0,6**	m
Z	0,53	0,96	**1,0**	m
L_T	1,23	1,13	**2,0**	m
L_B	0,79	0,87	**0,9**	m
Separator Wall Thickness				
Allowable Stress, S	122	mPa	17.7 ksi	(1 ksi = 6.895 mPa)
Welding Factor, E	1			
Temperature cofficient, y	0,4			
Corrosion Allowance, A	0,003			
	Bangma	**Lazalde -Crabtree**	**Spiral Inlet**	
Minimum thickness, tm	0,007	0,008	0,007	m
Overal height, H	2,01	2,00	2,90	m
Ellipse short radius, b	0,13	0,14	0,98	m
Ellipse long radius, a	0,26	0,29	0,26	m
Ellipse Surface Area	0,11	0,13	0,79	m2
Cylinder Surface Area	3,32	3,64	4,70	m2
Total Surface Area	3,43	3,77	5,49	m2
Volume of Steel, V	0,04	0,05	0,07	m3
Density of steel	7850			kg/m3
Weight of steel (rhoX volume)	341,84	375,63	547,55	kg
Cost/kg	2,94			USD/kg
Total Cost	1005,00	1104,34	1609,79	USD

Appendix Vc				
Separator Design Work Sheet - Case of SD2B unit				
Separation Pressure	1,2	mPa		
Steam Density@12bar	6,13	kg/m3		
Water Density@12bar	878,4	kg/m3		
Design Pressure CL150	2,0	mPa	(Design pressure for Class 150 = 20 bar)	
Mass flow rate steam, m	57,72	kg/s		
Volumetric flow rate, Qvs	9,42	m3/s		
Steam velocity (outlet)	40	m/s		
Flow Area, A	0,235	m3		
Diameter, Dt	0,547	m	Selected diameter DN550	
	Bangma	**Lazalde -Crabtree**	**Spiral Inlet**	
D	1,64	1,81	**1,6**	m
D_e	0,44	0,55	**0,5**	m
D_b	0,55	0,55	**0,4**	m
α	1,78	0,08	**0,2**	m
β	1,64	1,92	**1,8**	m
Z	1,64	3,01	**3,2**	m
L_T	3,83	3,54	**2,0**	m
L_B	2,46	2,72	**2,7**	m
Separator Wall Thickness				
Allowable Stress, S	122	mPa	17.7 ksi	(1 ksi = 6.895 mPa)
Welding Factor, E	1			
Temperature cofficient, y	0,4			
Corrosion Allowance, A	0,003			
	Bangma	**Lazalde -Crabtree**	**Spiral Inlet**	
Minimum thickness, tm	0,016	0,018	0,016	m
Overal height, H	6,30	6,27	4,72	m
Ellipse short radius, b	0,41	0,45	-1,29	m
Ellipse long radius, a	0,82	0,90	0,81	m
Ellipse Surface Area	1,06	1,28	-3,27	m2
Cylinder Surface Area	32,49	35,58	23,96	m2
Total Surface Area	33,54	36,86	20,69	m2
Volume of Steel, V	0,43	0,47	0,26	m3
Density of steel	7850			kg/m3
Weight of steel (rhoX volume)	3344,21	3674,76	2063,01	kg
Cost/kg	3,01			USD/kg
Total Cost	10066,09	11061,04	6209,67	USD

Appendix Vd				
Separator Design Work Sheet - Case of SD2c unit				
Separation Pressure	1,2	mPa		
Steam Density@12bar	6,13	kg/m3		
Water Density@12bar	878,4	kg/m3		
Design Pressure CL150	2,0	mPa	Design pressure for Class 150 = 20 bar	
Mass flow rate steam, m	36,19	kg/s		
Volumetric flow rate, Qvs	5,90	m3/s		
Steam velocity (outlet)	40	m/s		
Flow Area, A	0,148	m3		
Diameter, Dt	0,433	m	Selected diameter DN450	
	Bangma	**Lazalde -Crabtree**	**Spiral Inlet**	
D	1,30	1,43	**1,3**	m
D_e	0,35	0,43	**0,4**	m
D_b	0,43	0,43	**0,3**	m
α	1,41	0,07	**0,1**	m
β	1,30	1,52	**1,4**	m
Z	1,30	2,38	**2,5**	m
L_T	3,03	2,81	**2,0**	m
L_B	1,95	2,16	**2,1**	m
Separator Wall Thickness				
Allowable Stress, S	122	mPa	17.7 ksi	(1 ksi = 6.895 mPa)
Welding Factor, E	1			
Temperature cofficient, y	0,4			
Corrosion Allowance, A	0,003			
	Bangma	**Lazalde -Crabtree**	**Spiral Inlet**	
Minimum thickness, tm	0,014	0,015	0,013	m
Overal height, H	4,98	4,96	4,16	m
Ellipse short radius, b	0,33	0,36	-0,60	m
Ellipse long radius, a	0,65	0,72	0,64	m
Ellipse Surface Area	0,66	0,80	-1,20	m2
Cylinder Surface Area	20,37	22,31	16,73	m2
Total Surface Area	21,03	23,11	15,53	m2
Volume of Steel, V	0,27	0,29	0,20	m3
Density of steel	7850			kg/m3
Weight of steel (rho * volume)	2096,80	2304,05	1548,65	kg
Cost/kg	2,71			USD/kg
Total Cost	5682,32	6243,97	4196,84	USD

APPENDIX VI: Design results for the pipelines – both single-phase and two-phase flow pipes

Appendix VI - Pipline Design Work Sheet								
Pipe diameter								
Well	**908**	**908A**	**908B**	**910**	**910A**	**910B**	**909&909A**	
Separation Pressure	1,2	1,2	1,2	1,2	1,2	1,2	1,2	mPa
Steam Density@12bar	6,13	6,13	6,13	6,13	6,13	6,13	6,13	kg/m3
Water Density@12bar	878,4	878,4	878,4	878,4	878,4	878,4	878,4	kg/m3
Design Pressure CL150	2,0	2,0	2,0	2,0	2,0	2,0	2,0	mPa
(Design pressure for Class 150 = 20 bar =2.0 mpa)								
Mass flow rate steam, m	5,9	10	15,25	9,66	22,36	35,36	36,16	kg/s
Volumetric flow rate, Qvs	0,9625	1,6313	2,49	1,5759	3,6476	5,7684	5,8989	m3/s
Steam velocity (outlet)	40	40	40	40	40	40	40	m/s
Flow Area, A	0,0241	0,0408	0,0622	0,0394	0,0912	0,1442	0,1475	m3
Diameter, Dt	0,1750	0,2279	0,2814	0,2240	0,3407	0,4285	0,4333	m
Selected diameter(Do)	DN200	DN250	DN300	DN250	DN350	DN450	DN450	
Pipe Thickness Work Sheet								
1. Two-phase pipes	**908-SD2**	**908A-SD2**	**908B-SD2**	**910-SD2**	**910A-SD2**	**910B-SD2**	**9096909A-SD2**	
CL900 - 150 bar to take care of master valve P								
Design Pressure	15	15	15	15	15	15	15	mPa
Pipe Outer Diameter, D	0,2	0,25	0,3	0,25	0,35	0,45	0,45	m
Allowable Stress, S	122,00	122,00	122,00	122,00	122,00	122,00	122,00	mPa
Welding Factor, E	1	1	1	1	1	1	1	
Temperature cofficient, y	0,4	0,4	0,4	0,4	0,4	0,4	0,4	
Corrosion Allowance. A	0,003	0,003	0,003	0,003	0,003	0,003	0,003	m
Minimum Thickness, t (m)	0,0147	0,0176	0,0206	0,0176	0,0235	0,0294	0,0294	m
Minimum Thickness, t (mm)	14,72	17,65	20,58	17,65	23,51	29,37	29,37	mm
Selected Thickness (mm)	15,09	18,26	31,44	18,26	23,83	29,37	29,37	mm
Pipe OD (mm)	219,08	273,05	323,85	273,05	355,6	457,2	457,2	mm
Pipe ID (mm)	188,90	236,53	260,97	236,53	307,94	398,46	398,46	mm
Pipe OD (m)	0,21908	0,27305	0,32385	0,27305	0,3556	0,4572	0,4572	m
Pipe ID (m)	0,18890	0,23653	0,26097	0,23653	0,30794	0,39846	0,39846	m
Cost calculation								
Two phase pipe length	45,76	13,52	26,82	897,92	919,37	942,43	1654,46	m
Two-phase pipe steel volume	0,4426	0,1976	0,7747	13,1258	22,8380	37,2075	65,3187	m3
Steel Density	7850	7850	7850	7850	7850	7850	7850	kg/m3
Steel Mass (kg)	**3474,2**	**1551,4**	**6081,5**	**103037,8**	**179278,1**	**292078,9**	**512751,9**	kg/m3
Cost per kilogram (USD/Kg)	1,88	1,91	1,96	1,91	2,27	2,71	2,71	
Total cost/pipe line (USD)	**6.531**	**2.963**	**11.920**	**196.802**	**406.961**	**791.534**	**1.389.558**	**USD**
Total two-phase pipeline cost							**2.806.269**	

2. Single-phase pipes Steam	**SD2-OLK4**	**SD1-OLK4**	**SD3-OLK4**	**SD4-OLK4**	
CL150 - 20 bar std steam class					
Design Pressure	2	15	15	15	mPa
Pipe Outer Diameter, D	0,32	0,32	0,323	0,323	m
Allowable Stress, S	122,00	122,00	122	122	mPa
Welding Factor, E	1	1	1	1	
Temperature cofficient, y	0,4	0,40	0,4	0,4	
Corrosion Allowance. A	0,003	0,003	0,003	0,003	m
Minimum Thickness, t (m)	0,00563	0,02193	0,02193	0,02193	m
Minimum Thickness, t (mm)	5,63	21,93	21,93	21,93	mm
Selected Thickness (mm)	6,35	6,35	6,35	6,35	mm
Pipe OD (mm)	323,85	323,85	323,85	323,85	mm
Pipe ID (mm)	311,15	311,15	311,15	311,15	mm
Pipe OD (m)	0,32385	0,32385	0,32385	0,32385	mm
Pipe ID (m)	0,31115	0,31115	0,31115	0,31115	m
Brine Pipe length (m)	564	1421	930	1272	m
Brine pipe steel volume	3,573	9,002	5,891	8,058	m3
Steel Density	7850	7850	7850	7850	kg/m3
Steel Mass (kg)	28046,09471	70662,2351	46246,22	63252,89446	kg
Cost per kilogram (USD/Kg)	2,27	2,27	2,27	2,27	USD/kg
Total cost/pipe line (USD)	**63664,635**	**160403,274**	**104978,919**	**143584,0704**	USD
Total steam line cost				**408966,2635**	USD
3. Single-phase pipes brine					
CL900 - 150 bar std steam class	**SD2-911**	**SD2-911A**	**SD2-913**		
Design Pressure	15	15	15	mPa	
Pipe Outer Diameter, (Db)	0,10	0,4	0,3	m	
Allowable Stress, S	122,00	122,00	122,00	mPa	
Welding Factor, E	1	1	1		
Temperature cofficient, y	0,4	0,4	0,4		
Corrosion Allowance. A	0,003	0,003	0,003	m	
Minimum Thickness, t (m)	0,00886	0,02644	0,02058	m	
Minimum Thickness, t (mm)	8,86	26,44	20,58	mm	
Selected Thickness (mm)	11,53	30,96	21,44	mm	
Pipe OD (mm)	114	406,04	323,8	mm	
Pipe ID (mm)	92,04	344,48	280,92	mm	
Pipe OD (m)	0,114	0,40604	0,3238	m	
Pipe ID (m)	0,09204	0,34448	0,28092	m	
Brine Pipe length (m)	45,76	46,76	47,76	m	
Brine pipe steel volume	0,162636	1,696999	0,972791	m3	
Steel Density	7850	7851	7852	kg/m3	
Steel Mass (kg)	**1276,7**	**13323,1**	**7638,4**	kg	
Cost per kilogram (USD/Kg)	1,88	2,56	1,968	USD/kg	
Total cost/pipe line (USD)	**2.400**	**34.107**	**15.032**	USD	
Total Brine line cost			**51.540**	USD	